Immunity

The pre-exposure SARS-CoV-2-specific T cell repertoire determines the quality of the immune response to vaccination

Graphical abstract

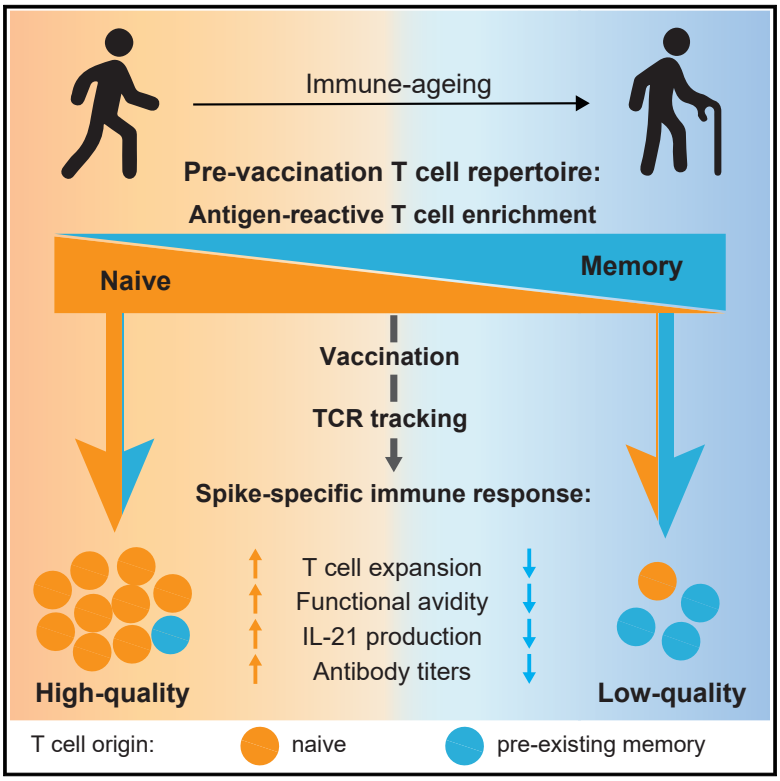

Highlights

- SARS-CoV-2-specific T cell expansion rate indicates immune-response quality
- Naive and memory pre-exposure repertoires inversely predict vaccine-response quality
- Pre-existing memory T cells are excluded from high-quality vaccination responses
- Impaired antigen-specific pre-exposure T cell repertoire as a hallmark of immune aging

Authors

Carina Saggau, Gabriela Rios Martini, Elisa Rosati, ..., Bimba Hoyer, Alexander Scheffold, Petra Bacher

Correspondence

p.bacher@ikmb.uni-kiel.de

In brief

Determinants of immune-response quality to SARS-CoV-2 remain poorly defined. Saggau et al. examine spike-specific naive and memory T cells pre- and post-vaccination and track pre-existing memory T cell receptors. They define T cell parameters of high-quality vaccine responses and identify high pre-existing memory and low naive T cell contributions as predictors of low-quality responses, particularly in the elderly.

Saggau et al., 2022, Immunity *55*, 1924–1939
October 11, 2022
https://doi.org/10.1016/j.immuni.2022.08.003

CellPress

CellPress

Immunity

Article

The pre-exposure SARS-CoV-2-specific T cell repertoire determines the quality of the immune response to vaccination

Carina Saggau,[1,14] Gabriela Rios Martini,[1,2,14] Elisa Rosati,[1,2,14] Silja Meise,[1] Berith Messner,[1,2] Ann-Kristin Kamps,[1,2] Nicole Bekel,[1,2] Johannes Gigla,[2] Ruben Rose,[3] Mathias Voß,[3] Ulf M. Geisen,[4] Hayley M. Reid,[4] Melike Sümbül,[5] Florian Tran,[2,6] Dennis K. Berner,[4] Yascha Khodamoradi,[7] Maria J.G.T. Vehreschild,[7] Oliver Cornely,[8,9,10,11] Philipp Koehler,[8,9,10] Andi Krumbholz,[3,12] Helmut Fickenscher,[3] Oliver Kreuzer,[13] Claudia Schreiber,[6] Andre Franke,[2] Stefan Schreiber,[2,6] Bimba Hoyer,[4] Alexander Scheffold,[1,14] and Petra Bacher[1,2,14,15,*]

[1]Institute of Immunology, Christian-Albrecht-University of Kiel, Arnold-Heller-Str. 3, Kiel, Schleswig-Holstein 24105, Germany

[2]Institute of Clinical Molecular Biology, Christian-Albrecht-University of Kiel, Rosalind-Franklin-Str. 12, Kiel, Schleswig-Holstein 24105, Germany

[3]Institute for Infection Medicine, Christian-Albrecht University of Kiel and University Medical Center Schleswig-Holstein, Campus Kiel, Kiel, Germany

[4]Medical Department I, Department for Rheumatology and Clinical Immunology, University Medical Center Schleswig-Holstein Campus Kiel, Kiel, Schleswig-Holstein, Germany

[5]Department of Dermatology, University Medical Center Schleswig-Holstein Campus Kiel, Kiel, Schleswig-Holstein, Germany

[6]Department of Internal Medicine I, University Medical Center Schleswig-Holstein Campus Kiel, Kiel, Schleswig-Holstein, Germany

[7]Department of Internal Medicine, Infectious Diseases, University Hospital Frankfurt & Goethe University Frankfurt, Frankfurt am Main, Germany

[8]University of Cologne, Faculty of Medicine and University Hospital Cologne, Department I of Internal Medicine, Center for Integrated Oncology Aachen Bonn Cologne Duesseldorf, Cologne, Germany

[9]University of Cologne, Faculty of Medicine and University Hospital Cologne, Translational Research, Cologne Excellence Cluster on Cellular Stress Responses in Aging-Associated Diseases (CECAD), Cologne, Germany

[10]University of Cologne, Faculty of Medicine and University Hospital Cologne, Center for Molecular Medicine Cologne (CMMC), Cologne, Germany

[11]German Centre for Infection Research (DZIF), Partner Site Bonn-Cologne, Cologne, Germany

[12]Labor Dr. Krause und Kollegen MVZ GmbH, Kiel, Germany

[13]Peptides & elephants GmbH, Hennigsdorf, Germany

[14]These authors contributed equally

[15]Lead contact

*Correspondence: p.bacher@ikmb.uni-kiel.de

https://doi.org/10.1016/j.immuni.2022.08.003

SUMMARY

SARS-CoV-2 infection and vaccination generates enormous host-response heterogeneity and an age-dependent loss of immune-response quality. How the pre-exposure T cell repertoire contributes to this heterogeneity is poorly understood. We combined analysis of SARS-CoV-2-specific CD4$^+$ T cells pre- and post-vaccination with longitudinal T cell receptor tracking. We identified strong pre-exposure T cell variability that correlated with subsequent immune-response quality and age. High-quality responses, defined by strong expansion of high-avidity spike-specific T cells, high interleukin-21 production, and specific immunoglobulin G, depended on an intact naive repertoire and exclusion of pre-existing memory T cells. In the elderly, T cell expansion from both compartments was severely compromised. Our results reveal that an intrinsic defect of the CD4$^+$ T cell repertoire causes the age-dependent decline of immune-response quality against SARS-CoV-2 and highlight the need for alternative strategies to induce high-quality T cell responses against newly arising pathogens in the elderly.

INTRODUCTION

Clinical symptoms of COVID-19 are highly diverse, ranging from no or mild symptoms to severe and often lethal disease, especially in the elderly. The rapid availability of highly effective SARS-CoV-2 vaccines is a cornerstone in the fight against the COVID-19 pandemic. However, vaccination efficacy is also variable and can be severely compromised in the elderly (Gustafson et al., 2020), as also observed following SARS-CoV-2 vaccination (Anderson et al., 2020; Collier et al., 2021; Li et al., 2021; Romero-Olmedo et al., 2022a). This is further indicated by more frequent break-through infections and an increased risk of developing severe symptoms in the elderly, even after full vaccination (Juthani et al., 2021; Wang et al., 2022; Yek et al., 2022). The

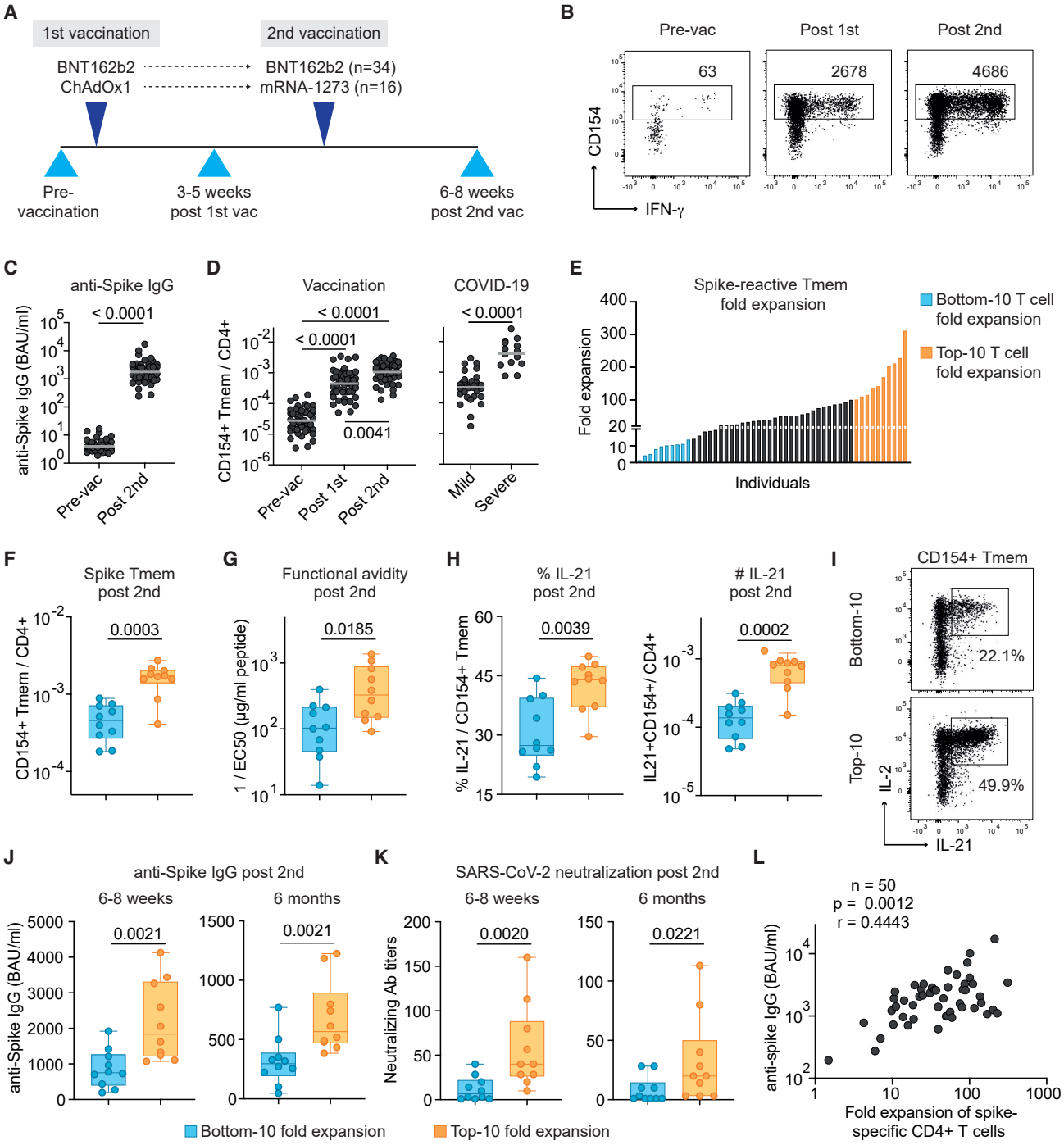

Figure 1. High- and low-quality CD4⁺ T cell responses develop upon SARS-CoV-2 vaccination

(A) Overview of the study design. Blood was drawn at the indicated time points and analyzed for SARS-CoV-2-specific CD4⁺ T cells and IgG. 34 individuals of our study received two doses of the BioNTech/Pfizer BNT162b2 mRNA vaccine, while 16 individuals received a heterologous immunization with AstraZeneca ChAdOx1 followed by Moderna mRNA-1273.

(B) Representative dot plot examples for the *ex vivo* detection of SARS-CoV-2 spike-reactive CD4⁺ T cells by ARTE pre- and post-vaccination. Absolute cell counts after magnetic CD154⁺ enrichment from 1x10e7 PBMCs are indicated.

(C) Serum anti-spike IgG antibody concentrations pre- and post-second vaccination.

(D) Frequencies of SARS-CoV-2 spike-reactive Tmems pre- and post-vaccination (left) in comparison to convalescent COVID-19 patients with mild (non-hospitalized) or severe disease (based on WHO criteria WHO4–7) (right).

(E) Vaccination-induced expansion of spike-reactive CD4⁺ Tmems was calculated for each donor based on the frequency pre-vaccination and after the second vaccination. Individuals with the lowest ("bottom 10") and highest ("top 10") expansion rate are indicated in blue or orange, respectively.

(legend continued on next page)

strong age association suggests that the immune status of the single individual is a critical component, which can also affect individuals from younger age groups. It is therefore a key question whether the antigen-specific pre-exposure status determines the quality of the response to SARS-CoV-2 vaccination, which would allow for identification of individuals at high risk and design of tailor-made protective measures.

$CD4^+$ T cells orchestrate adaptive immune responses, and the T cell compartment is dramatically affected by aging. Decreasing thymic activity leads to a reduced production of new naive T cells in the elderly. This may affect mainly the response to newly encountered antigens, as the T cell receptor (TCR) repertoire diversity providing specific high-affinity TCRs is reduced (Cicin-Sain et al., 2010; Gustafson et al., 2020; Woodland and Blackman, 2006; Yager et al., 2008). On the contrary, a broad memory repertoire accumulating with age can also provide T cells with specificities reactive to newly arising antigens (Woodland and Blackman, 2006). Such pre-existing memory T cells have been shown to result from cross-reactivity to related, or even unrelated, antigenic peptides (Birnbaum et al., 2014; Sewell, 2012). However, exaggerated clonal expansions, or increased numbers of senescent or chronically stimulated T cells lacking full proliferative and effector capacity, may negatively affect the response of pre-existing memory T cells (Allen et al., 2020). Thus, the composition and status of the antigen-specific pre-exposure T cell repertoire, comprising both a diverse naive compartment and certain pre-existing memory T cell specificities, forms a key determinant for the quality of the resulting immune response.

Pre-existing memory T cells against SARS-CoV-2 have been demonstrated in unexposed donors (Bacher et al., 2020; Braun et al., 2020; Grifoni et al., 2020; Le Bert et al., 2020; Mateus et al., 2020; Nelde et al., 2020). T cell cross-reactivity of these pre-existing SARS-CoV-2-reactive memory cells to related "common cold" corona viruses (CCCoVs) (Braun et al., 2020; Low et al., 2021; Loyal et al., 2021; Mateus et al., 2020; Nelde et al., 2020), but also other pathogens, has been described (Bacher et al., 2020; Bartolo et al., 2021; Stervbo et al., 2020; Tan et al., 2021). Importantly, pre-existing T cell memory against so far unexposed antigens is a common phenomenon for many antigens (Bacher et al., 2013; Campion et al., 2014; Kwok et al., 2012; Pan et al., 2021; Su et al., 2013). So far, it is still not clear to what extent pre-existing memory T cells contribute to the immune response against SARS-CoV-2 and how they influence the response quality. Several studies find correlations between the frequency of SARS-CoV-2-reactive pre-existing memory cells and mild or asymptomatic COVID-19 or improved immunity to vaccination (Loyal et al., 2021; Mallajosyula et al., 2021; Mateus et al., 2021; Swadling et al., 2022). We and others recently detected pre-existing memory T cells against SARS-CoV-2 in essentially all unexposed individuals (Bacher et al., 2020; Guerrera et al., 2021). These cells display rather low functional avidity to SARS-CoV-2 (Bacher et al., 2020), which was confirmed even for major conserved peptide epitopes between SARS-CoV-2 and CCCoVs (Dykema et al., 2021). Low-avidity $CD4^+$ T cells are also a hallmark of severe COVID-19, suggesting their potential recruitment from the pre-existing memory compartment (Bacher et al., 2020). These data challenge the idea of a protective contribution of pre-existing memory $CD4^+$ T cells to SARS-CoV-2 immunity and even suggest a potential negative impact on the immune-response quality. However, as of yet, the quantitative contribution of pre-existing memory T cells and their impact on the response quality has not been directly assessed.

Here, we employed antigen-reactive T cell enrichment (ARTE) (Bacher et al., 2013, 2016, 2019, 2020) in combination with clonal TCR tracking to follow the fate of pre-existing memory T cells and to characterize naive and memory SARS-COV-2-specific T cells pre- and post-vaccination. We identified the pre-vaccination repertoire as a major determinant for the immune-response quality to vaccination. Strong clonal expansion, but exclusion of pre-existing memory T cells, was a hallmark of high-quality immune responses, which were characterized by high frequencies of high-avidity spike-specific T cells, strong interleukin-21 (IL-21) production, and higher concentration of anti-spike immunoglobulin G (IgG). Age-related changes in both the naive and memory pre-exposure T cell repertoire resulted in a $CD4^+$ T cell-intrinsic inability to mount high-quality immune responses in the elderly (>80 years), emphasizing the need for novel intervention strategies.

RESULTS

SARS-CoV-2 vaccination generates qualitatively different $CD4^+$ T cell responses

We analyzed the SARS-CoV-2 spike protein-specific $CD4^+$ T cell response before and after vaccination in 50 SARS-CoV-2-naive individuals, which was confirmed by testing negative for SARS-CoV-2 IgG pre-vaccination (Figure S1A). Three donors became infected with SARS-CoV-2 during the course of our study, as indicated by an increase in nucleocapsid protein-specific IgG, and were excluded from further analysis (Figure S1A). Blood was drawn pre-vaccination, 3–5 weeks after the first vaccination, and 6–8 weeks after the second vaccination (Figure 1A).

To analyze the whole repertoire of spike-specific $CD4^+$ T cells, including memory and naive cells, we used a previously developed highly sensitive technology, the ARTE assay (Bacher et al., 2013, 2016, 2019, 2020). Freshly isolated peripheral blood mononuclear cells (PBMCs) were stimulated *ex vivo* for 7 hours with a peptide pool spanning the whole spike-protein sequence.

(F) Bottom 10 and top 10 expanders were determined as described in (E) and compared for spike-reactive Tmem frequencies.
(G) Spike-reactive $CD154^+$ Tmems were FACS-purified, expanded, and re-stimulated with decreasing antigen concentration in the presence of autologous antigen-presenting cells. Reactive cells were determined by re-expression of CD154 and TNF-α, and EC50 values were calculated from dose-response curves.
(H) *Ex vivo* IL-21 production of spike-reactive T cells, within $CD154^+$ Tmems (left) or within total $CD4^+$ T cells (right).
(I) Dot plot example of spike-specific IL-21 and IL-2 production of a bottom 10 or top 10 donor.
(J and K) Anti-spike IgG concentrations (J) and SARS-CoV-2 serum neutralization titers (K) at 6–8 weeks and 6 months post-second vaccination.
(L) Spearman correlation of the fold expansion of spike-reactive $CD4^+$ T cells and anti-spike IgG concentrations measured 6–8 weeks post-second vaccination.
Each symbol in (C, D, F–H, J–L) represents one donor; horizontal lines indicate geometric mean in (C, D). Box-and-whisker plots display quartiles and range in (F–H, J, K). Statistical differences: Friedman test with Dunn's post hoc test in (D, left); two-tailed Mann-Whitney test in (D, right) and (C, F–H, J, K). See also Figures S1–S3.

Spike-reactive CD4$^+$ T cells were detected based on up-regulation of CD154 (CD40L) and magnetically enriched from 1×10e7 PBMCs. This enabled a precise enumeration of rare spike-reactive T cells pre-vaccination (Figures 1B and S1B) with a minimum of 50 detected CD154$^+$ cells (range 50–689, mean 166) after subtraction of background events (Figures S1C and S1D), which allowed detection of spike-reactive pre-vaccination responses in both the naive repertoire and from cross-reactive pre-existing memory cells (Figures S1B–S1D). Specificity of CD154$^+$ cells pre- and post-vaccination was confirmed by expansion of sorted CD154$^+$ memory T cells followed by restimulation with spike peptide pool or a negative control pool of influenza A proteins (Figure S1E), as reported previously (Bacher et al., 2020). Most donors of our study (n = 34) received two doses of the BioNtech/Pfizer BNT162b2 mRNA vaccine, while 16 individuals received a heterologous immunization with AstraZeneca ChAdOx1, followed by Moderna mRNA-1273 (Figure 1A and Tables S1 and S2). We observed no significant differences in the frequencies of spike-reactive CD4$^+$ T cells or anti-spike IgG concentrations between these two vaccination regimens (Figures S1F and S1G).

Vaccination induced spike-specific IgG (Figure 1C) as well as spike-reactive memory CD4$^+$ T cells (Tmems) at magnitudes comparable to those observed in convalescent COVID-19 patients with mild disease (Figure 1D). As expected, the post-vaccine response was characterized by a shift from naive to memory cells, especially of the effector memory phenotype (CD45RA$^-$CCR7$^-$) (Figure S2A). Analysis of recent *in vivo* activation showed increased CD38 expression post-first vaccination that declined thereafter (Figure S2A). The post-vaccination response was further characterized by increased frequencies of IL-2-, IFN-γ-, IL-21-, and IL-10-producing cells (Figure S2B) that were in a similar range as in convalescent COVID-19 patients (Bacher et al., 2020).

To identify potential differences in the host-response quality, we calculated the SARS-CoV-2 spike-specific T cell expansion for each donor based on the frequencies pre-vaccination and post-second vaccination. The fold expansion displayed strong differences between individuals, ranging from a 2- to 312-fold increase in spike-reactive Tmems (Figure 1E). We next compared the bottom 10 expanders (≤15-fold expansion) and top 10 expanders (≥100-fold expansion) (Figure 1E). Donors contained in the top 10 group not only reached higher frequencies of spike-reactive Tmems (Figure 1F), but also had cells with a higher functional avidity (Figure 1G), as tested by restimulation of expanded spike-specific T cells with graded antigen concentrations (Figure S2C). Furthermore, top 10 expanders showed significantly increased IL-21 production (Figures 1H and 1I) but similar frequencies of IFN-γ, IL-2, or IL-10 producers (Figure S3D). Because IL-21 is an essential cytokine for B cell help, we next analyzed anti-spike IgG antibodies. Top 10 expanders displayed higher concentrations of anti-spike IgG (Figure 1J) as well as higher titers of SARS-CoV-2-neutralizing antibodies (Figure 1K). In line with these results, we observed a strong positive correlation between the fold expansion of spike-specific CD4$^+$ T cells and anti-spike IgG concentrations (Figure 1L) or neutralizing antibody titers (Figure S3A) as well as the frequency of IL-21 producers (Figure S3B). The differences in anti-spike antibodies were also retained 6 months after the second vaccination (Figures 1J and 1K), although anti-spike IgG concentrations generally declined in all donors.

Overall, these data identify strong qualitative differences in the CD4$^+$ T cell response to SARS-CoV-2 between individual vaccinees. A high-quality immune response is characterized by strong T cell expansion, resulting in high frequencies of high-avidity T cells and high IL-21 production, which correlates with high concentrations of anti-spike IgG antibodies.

High age predisposes individuals for poor T cell expansion despite increased pre-existing memory

We next asked which parameters might influence these qualitative differences between individuals. Vaccination efficacy is known to decline with age (Gustafson et al., 2020), and indeed the bottom 10 group contained a higher proportion of individuals >80 years of age (Figure 2A). Pre-existing T cell memory against SARS-CoV-2 in unexposed donors has been described, but its impact on infection and vaccination is controversially discussed (Moss, 2022). When we compared the frequencies of spike-specific memory cells before vaccination or the proportion of memory cells within the spike-specific T cells, we observed much higher frequencies of pre-existing memory T cells in the bottom 10 compared with the top 10 expander group (Figures 2B and 2C and Figure S3C). This is in line with our previous results, showing that pre-existing memory frequencies increase with age and correlate with the relative proportion of memory cells within the total CD4$^+$ T cells, reflecting the cumulative immunological experience of an individual (Bacher et al., 2020).

To determine the potential impact of age and pre-existing memory in more detail, we compared different age groups within our cohort. Representative young (<25 years) and old (>80 years) individuals are depicted in Figure 2D, highlighting that the proportion of spike-reactive memory versus naive T cells recapitulates the memory-naive distribution in the total CD4$^+$ T cell compartment (Figure 2D), as shown before (Bacher et al., 2020). Overall, the frequency of pre-existing memory T cells was variable between individuals but tended to increase with age and was particularly high in donors >80 years of age (Figure 2E). However, upon vaccination, spike-specific T cells poorly expanded in this age group, as shown for the representative young and old donor (Figure 2F) as well as for the whole cohort (Figure 2G). Consistent with this, the >80 years age group had the lowest frequency of spike-specific T cells post-vaccination (Figure 2H), as well as the lowest anti-spike IgG concentrations and SARS-CoV-2-neutralizing antibody titers (Figures 2I and 2J), despite having started with the highest frequencies of pre-existing memory cells pre-vaccination (Figure 2E). Spike-specific CD4$^+$ T cells remained low even after the third vaccination in the >80 years age group, in contrast to anti-spike IgG antibodies, which reached similar concentrations as in the other age groups (Figures 2H and 2I). Thus, donor age has a strong negative influence on T cell response quality despite high frequencies of pre-existing memory T cells.

High pre-existing memory and a low proportion of naive T cells predict poor T cell responses

High pre-existing memory T cell frequencies were mainly found in the elderly, but not exclusively (Figure 2E). We therefore

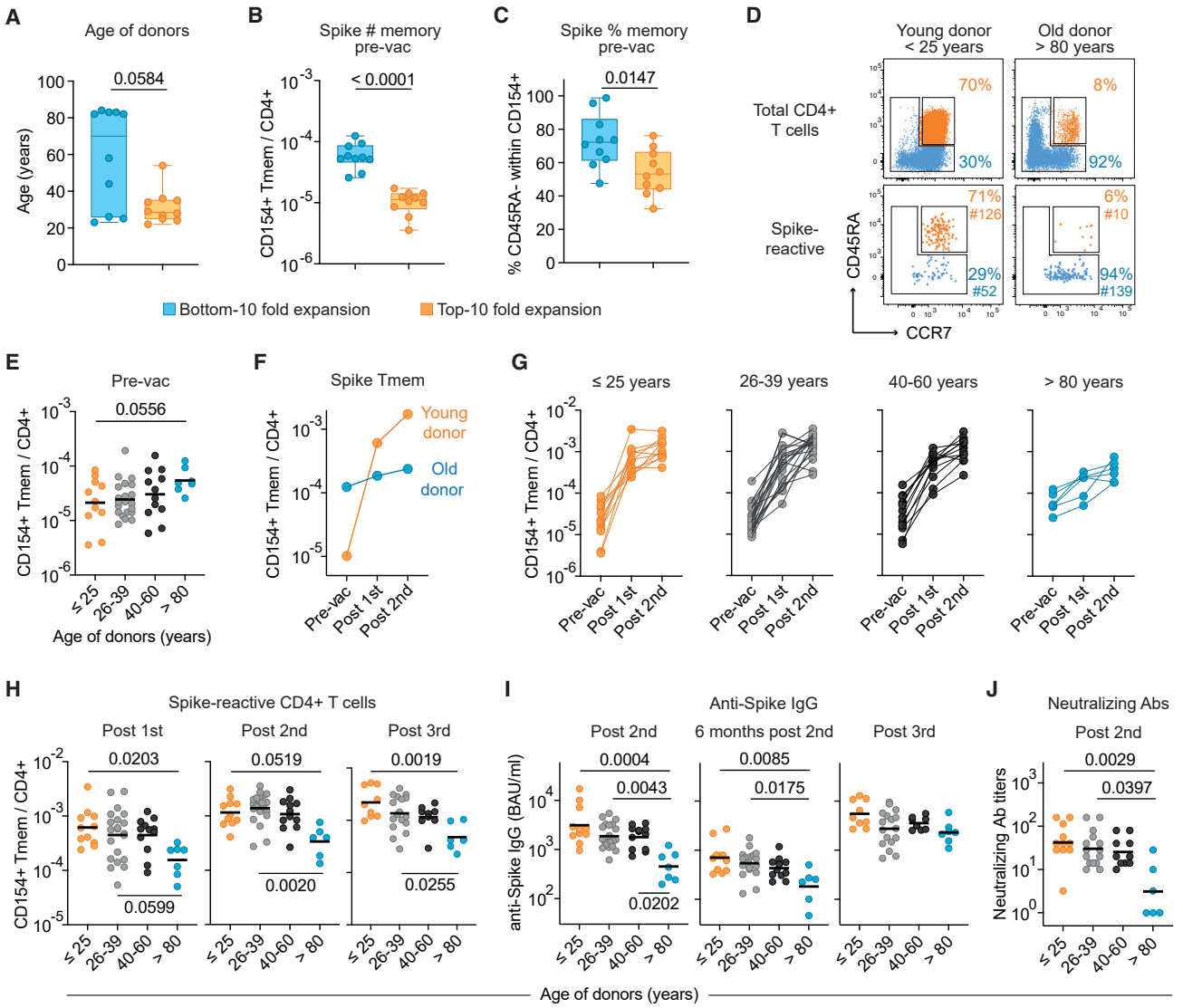

Figure 2. The spike-specific immune response declines with age

(A–C) Bottom 10 and top 10 expanders were determined as described in Figure 1E and analyzed for (A) age, (B) frequencies of SARS-CoV-2 spike-reactive Tmem pre-vaccination, and (C) the proportion of CD45RA$^-$ Tmem cells within spike-reactive cells pre-vaccination.

(D) Representative CD45RA and CCR7 staining of total CD4$^+$ T cells (upper plots) and spike-reactive CD154$^+$ cells pre-vaccination of a young (<25 years) and old (>80 years) individual. Percentages of naive and memory cells and absolute cell counts of enriched spike-reactive T cells are indicated.

(E) Frequencies of spike-reactive memory cells pre-vaccination in different age groups.

(F) Vaccination-induced expansion of spike-reactive memory cells in the two representative donors from (D).

(G) Vaccination-induced expansion of spike-reactive memory cells in different age groups. (≤25, n = 11; 26–39, n = 21; 40–60, n = 12; >80, n = 6).

(H) Frequencies of spike-reactive CD4$^+$ Tmems post-first, post-second, or post-third vaccination in different age groups.

(I) Serum anti-spike IgG concentrations 6–8 weeks or 6 months post-second vaccination or post-third vaccination in different age groups.

(J) SARS-CoV-2 serum neutralization titers 6–8 weeks post-second vaccination. Each symbol in (A–C) and (E–J) represents one donor; box-and-whisker plots display quartiles and range in (A–C). Horizontal lines indicate geometric mean in (E, H, I, J). Statistical differences: two-tailed Mann-Whitney test in (A–C); Kruskal-Wallis test with Dunn's post hoc test in (E, H, I, J). See also Figure S3.

analyzed whether pre-existing memory is an independent predictor of the T cell response quality. To dissect the role of pre-existing memory independently of the effects of high age, the >80 years group was depicted separately. Indeed, the Tmem frequency showed a strong negative correlation with the fold expansion of spike-specific T cells (Figure 3A), which was confirmed for each individual age group (Figure S3D). This was also obvious when donors were divided into several bins based on increasing numbers of pre-existing memory cells (Figure 3B). Accordingly, donors with the lowest frequencies of pre-existing memory showed the highest production of IL-21 (Figure 3C) and a tendency toward higher functional avidity, although not statistically significant (Figure 3D). These data indicate that pre-existing memory T cells expand poorly upon SARS-CoV-2

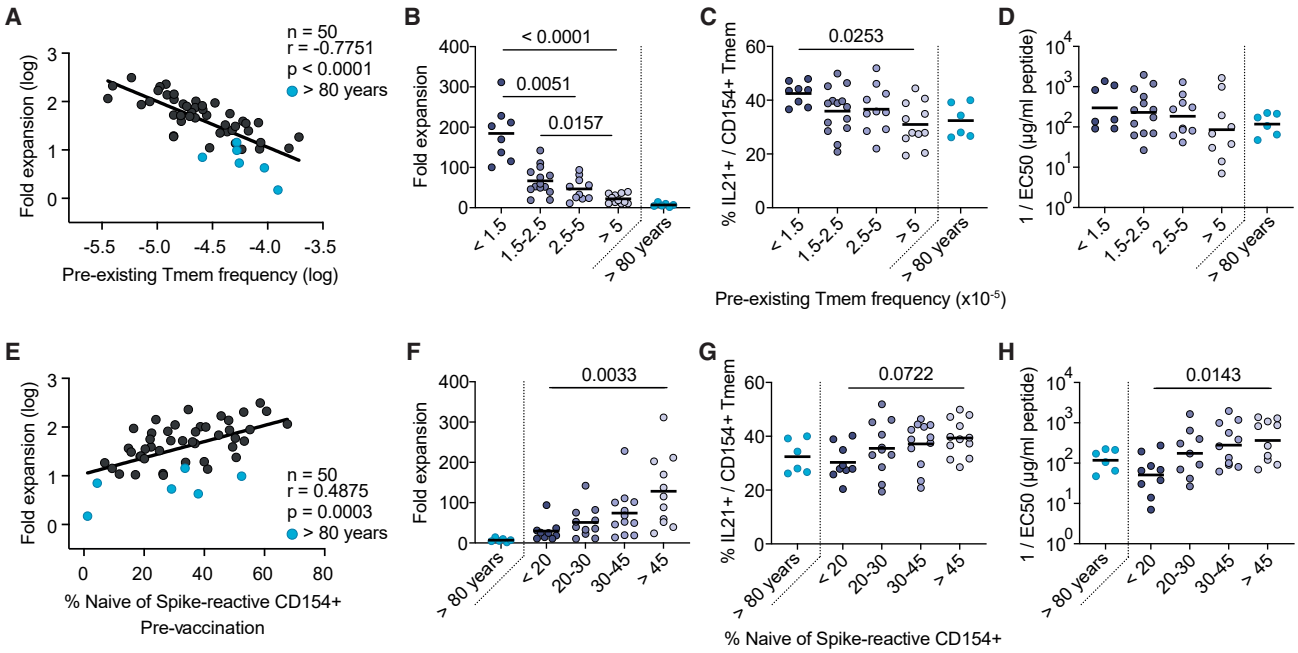

Figure 3. Pre-existing memory cells expand poorly upon vaccination

(A) Spearman correlation between the frequencies of spike-reactive Tmems pre-vaccination (x axis) and the fold expansion post-second vaccination (y axis). (B–D) Donors were grouped by their pre-vaccination frequencies of spike-reactive Tmems (<1.5, n = 8; 1.5–2.5, n = 14; 2.5–5, n = 10; >5, n = 11). Donors >80 years of age (n = 6) are depicted as separate group. For each bin, the (B) fold expansion post-second vaccination, (C) percentage of IL-21 production within $CD154^+$ Tmems, and (D) functional avidity of expanded spike-reactive T cells is indicated.

(E) Spearman correlation between the proportion of spike-reactive naive cells pre-vaccination (x axis) and the fold expansion post-second vaccination (y axis). (F–H) Donors were grouped by their pre-vaccination proportion of spike-reactive naive cells (<20, n = 9; 20–30, n = 11; 30–45, n = 12; >45, n = 11). Donors >80 years of age (n = 6) are depicted as separate group. For each bin, the (F) fold expansion post-second vaccination, (G) percentage of IL-21 production within $CD154^+$ Tmems, and (H) functional avidity of expanded spike-reactive T cells is indicated. Each symbol in (A–H) represents one donor; horizontal lines indicate mean in (B, C, F, G) and geometric mean in (D, H). Statistical differences: Kruskal-Wallis test with Dunn's post hoc test in (B–D, F–H). To determine differences between the younger age groups, donors >80 years of age were excluded from statistical analysis. See also Figure S3.

vaccination but also suggest that additional parameters may determine the selection of high-avidity T cells.

SARS-CoV-2-specific T cells within the naive pre-vaccination repertoire have so far not been analyzed, but the high sensitivity of the ARTE technology allows us to do this. In general, we observed a negative correlation between the frequencies of pre-existing memory cells and the percentage of naive cells within the spike-reactive pre-vaccination T cell pool (Figure S3E). Furthermore, the proportion of spike-reactive naive T cells showed a positive correlation with the expansion rate following vaccination (Figures 3E and 3F). The pre-vaccination naive pool size also correlated with IL-21 production (Figure 3G) as well as the functional avidity of spike-specific T cells post-vaccination (Figure 3H). Indeed, frequencies of IL-21 producers and high-avidity responses significantly dropped when the proportion of pre-vaccination spike-specific naive T cells was below 20% (Figures 3G and 3H). These data suggest that high-avidity T cells with high expansion potential are preferentially recruited from the naive compartment.

Overall, our data indicate that the vaccination success, defined by formation of a highly expanded, IL-21-producing, high-avidity T cell pool, is predicted by two interdependent, but not strictly linked, parameters: the frequency of pre-existing spike-specific memory T cells, mainly determined by the immunological experience of an individual, and the proportion of naive T cells within the pre-vaccination spike-specific T cell pool determined by thymic activity.

Pre-existing memory T cell clonotypes minimally contribute to high-quality T cell responses

Our results so far contradict the expectation that pre-existing memory T cells support immune responses against SARS-CoV-2 vaccination. To directly assess the contribution of pre-existing memory cells to the post-vaccination repertoire, we performed clonal TCR tracking using TCR sequencing from *ex vivo* sorted spike-reactive memory T cells from 37 donors pre- and post-vaccination (Table S3). Consistent with their predicted low expansion capacity, pre-existing memory TCR-β chains accounted on average for 6.1% of the top 100 clonotypes post-vaccination, while most of the post-vaccination clonotypes were not detected at baseline (Figure 4A). Also, the cumulative abundance of pre-existing clonotypes contributing to the top 100 post-vaccination repertoire was on average only 10%. However, in two donors, pre-existing clonotypes made up more than 25% of the post-vaccination repertoire (Figure 4A). Analysis of the TCR-α repertoire showed similar results (Figure S4A). Next, we used the TCRdist algorithm to identify closely related clonotypes based on shared CDR3 sequence features (Dash et al.,

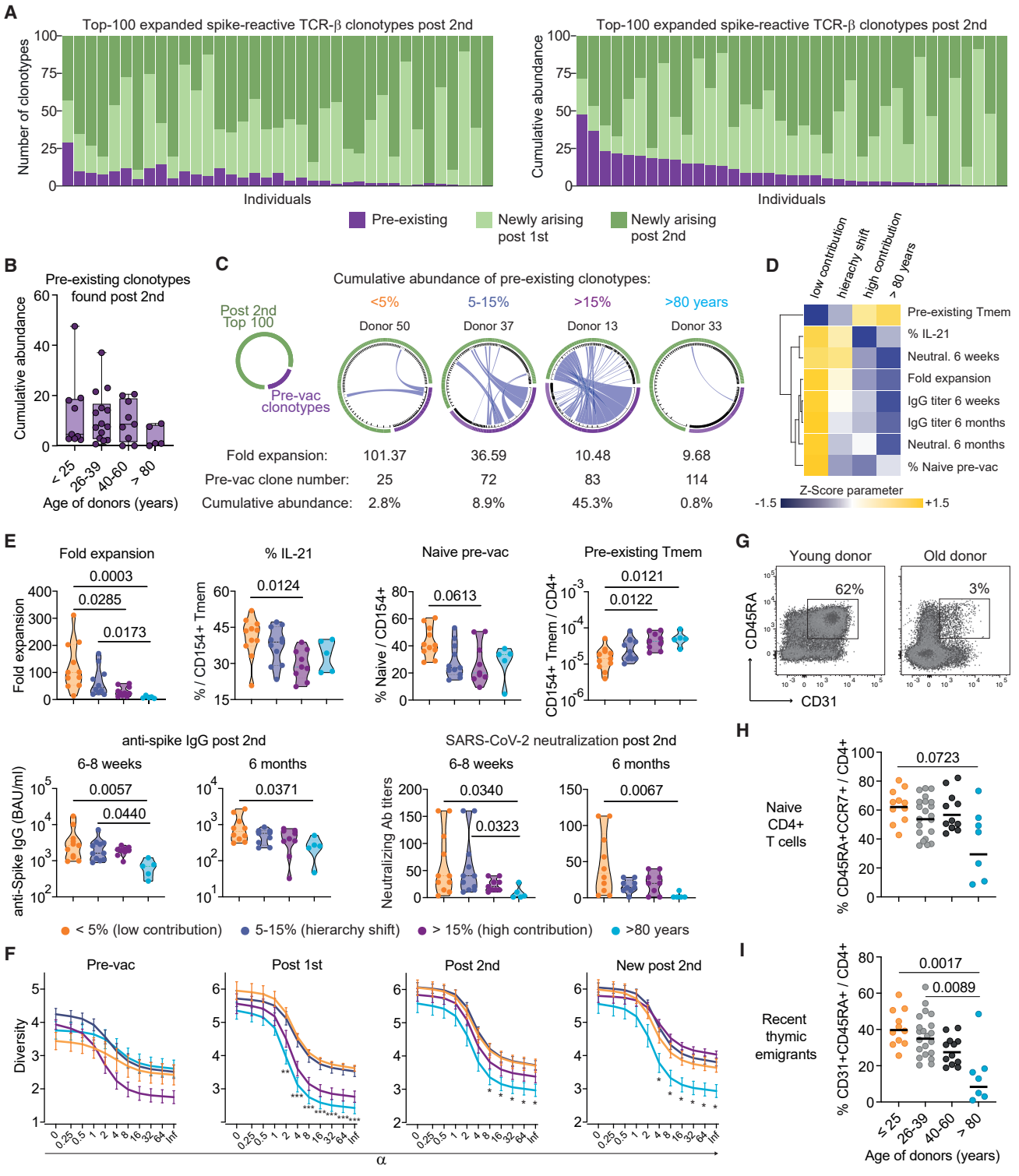

Figure 4. TCR sequencing post-vaccination identifies primarily newly arising clonotypes

(A–C) Spike-reactive memory T cells were *ex vivo* sorted pre- and post-vaccination and analyzed by bulk TCR sequencing. Analysis of the top 100 expanded TCR-β spike-reactive clonotypes post-second vaccination is shown.

(A) The number of clonotypes (left graph) and their cumulative relative abundance (right graph) derived from the pre-existing, post-first or post-second vaccination repertoire is indicated. Each bar represents one donor (n = 37).

(B) Cumulative abundance of pre-existing or newly arising clonotypes found in the top 100 TCR repertoire post-second vaccination for different age groups (>25, n = 9; 26–39, n = 14; 40–60, n = 9, >80, n = 5).

(legend continued on next page)

2017; Schattgen et al., 2022). We identified several spike-reactive meta-clonotypes within our dataset (Figures S4B and S4C and Table S3) and also re-identified public immunodominant clusters previously reported in COVID-19 patients and SARS-CoV-2 vaccinees (Mudd et al., 2022; Rosati et al., 2021), confirming the spike specificity of our clonotypes. Also, within the biggest similarity clusters, most clonotypes were newly arising, while pre-existing clonotypes belonging to these clusters were only found in individual donors (Figure S4D).

Since the frequencies of pre-existing memory cells were particularly elevated in the elderly (Figure 2E), we next compared the recruitment of pre-existing clonotypes into the vaccine response in the different age groups (Figure 4B). There was no significant difference between age groups, and unexpectedly, the >80 years group showed a rather low contribution of pre-existing memory clonotypes to the post-vaccine response despite having the highest frequencies before vaccination (Figure 4B).

To better define the pre-existing memory dynamics, we analyzed the clonal fate in each individual donor. Clonal fate tracking is displayed as circos plots showing clonotypes pre-vaccination and the top 100 clonotypes post-second vaccination. Connecting lines show TCR-β sequences that are present at both time points, and the width of the connecting line indicates the relative size of each clone in the pre- or post-vaccination repertoire, respectively (Figures 4C and S5). Grouping donors according to the cumulative abundance of pre-existing clonotypes in the post-vaccination repertoire (<5%, 5–15%, >15%) (Figure S5A) correlated with three different response patterns (Figures 4D and 4E). In the "low contribution" group, the abundance of pre-existing clonotypes in the post-vaccination repertoire is negligible (<5%), whereas in the "hierarchy shift" group (5–15%), strongly expanded clonotypes pre-vaccination represent rather subdominant clonotypes post-vaccination. Thus, the T cell response in these groups is dominated by newly arising, strongly expanding clonotypes, most likely from the naive compartment. In contrast, in the third, "high contribution" group (>15%), strongly expanded pre-existing memory clonotypes remain dominant post-vaccination, suggesting a low contribution of newly arising clonotypes. Donors >80 years of age mainly fell into the low contribution group, but to enable differentiation between age and pre-existing memory-mediated effects, they are further depicted separately.

Within these different response patterns, we next analyzed the independently assessed spike-specific vaccine-response quality parameters (Figures 4D and 4E). The low contribution group had the highest T cell fold expansion, as well as high IL-21 production after vaccination, while showing the highest proportion of spike-reactive naive cells and the lowest frequencies of pre-existing memory cells pre-vaccination (Figures 4D and 4E). Furthermore, high and more stable concentrations of anti-spike IgG and SARS-CoV-2-neutralizing antibodies were found in this group (Figure 4E). Despite a tendency toward a slight quality loss, the hierarchy switch group was most similar to the low contribution group, indicating an overall high-quality vaccine response. In contrast, the high contribution group showed a significant decline in several quality parameters, such as low fold expansion, low IL-21, and a tendency toward reduced IgG stability while having a high frequency of pre-existing memory cells. The high contribution group was in many parameters not statistically different from the >80 years group, which displayed uniformly poor response quality (Figure 4E).

These data support the hypothesis that a diverse naive compartment, allowing the selection of high-affinity T cells, is required for high-quality SARS-CoV-2 T cell responses rather than pre-existing memory T cells. To better quantitate this effect, we analyzed the TCR diversity pre- and post-vaccination. The diversity of pre-existing memory before vaccination was not different between the groups. However, especially after the first, but also after the second, vaccination, a diverse SARS-CoV-2-specific repertoire developed in the low contribution and hierarchy switch groups, consistent with recruitment of multiple clonotypes from a diverse naive repertoire. In contrast, the high contribution group, and in particular the ">80 years" donors, displayed a lower TCR diversity (Figure 4F). Also, when only analyzing the newly arising clonotypes, the >80 years group still had a reduced diversity, suggesting a limited and poorly expanding naive pre-vaccination repertoire in the elderly. This is further supported by a strong reduction of the naive T cell pool

(C) Each circos plot represents the TCR-β sequences of the detected clonotypes pre-vaccination and the top 100 clonotypes post-second vaccination of one donor. Connecting lines show TCR-β sequences that are present at both time points. The fold expansion, the absolute number of clonotypes detected pre-vaccination, and the cumulative abundance of pre-existing clonotypes in the post-vaccine repertoire are indicated for each representative donor.

(D) Donors were grouped according to the cumulative abundance of pre-existing clonotypes in the top 100 post-vaccination repertoire (<5%, n = 11; 5–15%, n = 11; >15%, n = 9; donors >80 years of age, n = 5). Mean values for the indicated parameters were calculated, *Z* score normalized for each parameter and are shown as heatmap.

(E) Donors were grouped as described in (D) and the fold expansion, IL-21 production within $CD154^+$ Tmems, the proportion of spike-reactive naive T cells pre-vaccination, the frequencies of pre-existing Tmems, and anti-spike IgG concentrations or SARS-CoV-2 serum neutralization titers post-second vaccination are indicated.

(F) Rényi diversity profiles were calculated for mean values of the different pre-existing memory bins (<5%, n = 11; 5–15%, n = 11; >15%, n = 9; >80y, n = 5). By varying the scaling parameter α, different diversity indices are calculated. At values of 0, 1, 2, and infinite richness, Shannon diversity, Simpson diversity, and Berger-Parker index are calculated (see STAR Methods). Thus, the sample with the highest value at $\alpha = 0$ has the highest richness, i.e., highest number of clonotypes, but the lower value at α = infinite indicates a higher proportion of the most abundant TCRs, i.e., lower population diversity. A sample with a profile that is overall higher than the profiles of other samples is therefore more diverse. Diversity of the total spike-specific TCR-β repertoire pre-vaccination, post-first, and post-second vaccination as well as of the newly arising clonotypes post-second vaccination are shown.

(G) Representative CD45RA and CD31 staining of a young and old individual.

(H) Proportion of naive ($CD45RA^+CCR7^+$) within total $CD4^+$ T cells in different age groups.

(I) Proportion of RTE ($CD45RA^+CD31^+$) within total $CD4^+$ T cells in different age groups. Each symbol in (B, E, H, I) represents one donor. Box-and-whisker plots display quartiles and range in (B); truncated violin plots with quartiles and range are shown in (E). Symbols and error bars indicate mean and SEM in (F). Horizontal lines indicate mean in (H, I). Statistical differences: Kruskal-Wallis test with Dunn's post hoc test in (E, F, H, I). See also Figures S4 and S5.

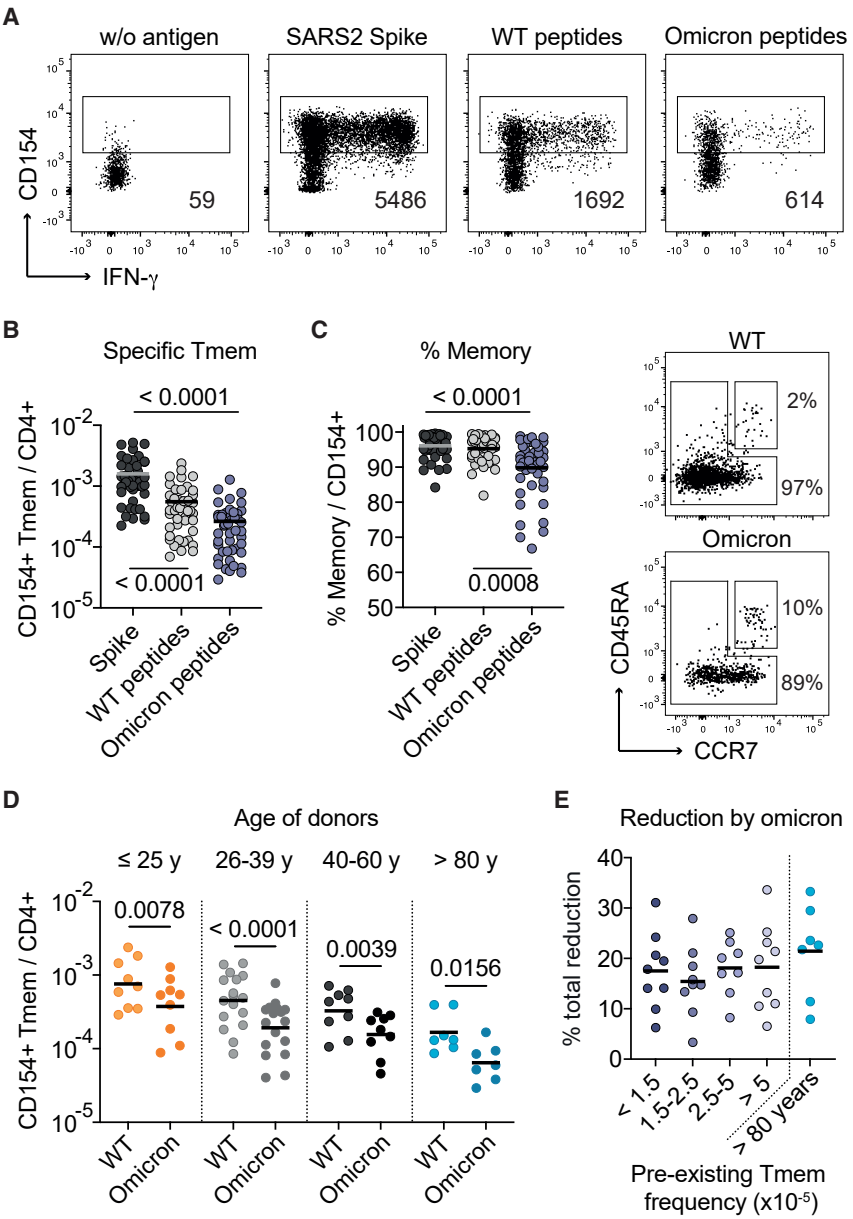

Figure 5. T cell reactivity against SARS-CoV-2 Omicron varies between individuals

(A) Representative dot plot examples showing antigen-reactive T cells against the full-length spike, a pool of 80 peptides affected by the Omicron B.1.1.529 BA.1 mutations (Omicron peptides), and the corresponding wild-type peptides from one donor. Absolute cell counts after magnetic CD154$^+$ enrichment from 1x10e7 PBMCs are indicated.

(B) Frequencies of reactive CD4$^+$ memory T cells against the indicated antigens analyzed post-third vaccination (n = 45).

(C) Proportion of CD45RA$^-$ memory T cells within reactive CD154$^+$CD4$^+$ T cells (n = 45) and representative CD45RA and CCR7 staining for the wild-type and Omicron peptide-reactive T cells.

(D) Frequencies of reactive CD4$^+$ Tmems against the wild-type and Omicron peptides analyzed post-third vaccination in different age groups (<25, n = 9; 26–39, n = 17; 40–60, n = 9; >80, n = 7).

(E) Donors were grouped by their pre-vaccination frequencies of spike-reactive Tmems as described in Figure 3, and the percentage of total reduction in spike-specific T cells by the Omicron peptides is depicted. Each symbol in (B–E) represents one donor; horizontal lines indicate mean in (B, C, E) and geometric mean in (D). Statistical differences: Kruskal-Wallis test with Dunn's post hoc test in (B–D).

and in particular of recent thymic emigrants (RTEs), especially in individuals >80 years of age (Figures 4G–4I), which is a well-known mechanism of immune aging (Mittelbrunn and Kroemer, 2021).

In summary, these data indicate how the contribution of pre-existing memory and naive T cells differentially affects the immune-response quality following vaccination and how this may be altered upon aging. High-quality immune responses were in general connected to a low contribution of pre-existing memory and a dominant contribution of newly arising clonotypes with the capacity to strongly expand. In contrast, pre-existing memory T cells seem to have low proliferative potential, leading to low-quality responses if not compensated, e.g., from the naive pool, like in the hierarchy shift group. This is particularly evident in the >80 years group, which showed a loss of proliferative capacity in the pre-existing memory, as well as reduced TCR diversity in the newly arising clonotypes, suggesting impaired recruitment from a reduced naive compartment.

The decline in T cell reactivity against the Omicron variant is variable between individuals

T cell responses are less affected by virus variants, such as Omicron B.1.1.529, compared with antibody responses due to the recognition of many different epitopes. However, low-quality T cell responses with restricted TCR diversity may be particularly at risk. We therefore analyzed the response against 80 selected spike peptides affected by Omicron B.1.1.529 BA.1 mutations ("Omicron peptides") and their corresponding "wild-type peptides" (Figure 5A and Table S4). In vaccinated donors, the wild-type peptide pool accounted on average for 30% of the T cell response against the total spike protein and was further decreased by an average of 50% against the Omicron peptides (Figure 5B). The Omicron peptides stimulated a higher fraction of naive T cells (Figure 5C), as expected, due to sequence changes arising by the mutations, resulting in new T cell epitopes not being present in the wild-type spike used for vaccination (see Table S4).

In line with our previous results, T cell reactivity against the wild-type and Omicron peptides declined with donor age (Figure 5D). However, we did not observe a particular decline in the >80 years group, nor in individuals with a high contribution of pre-existing memory, but rather we observed high variability

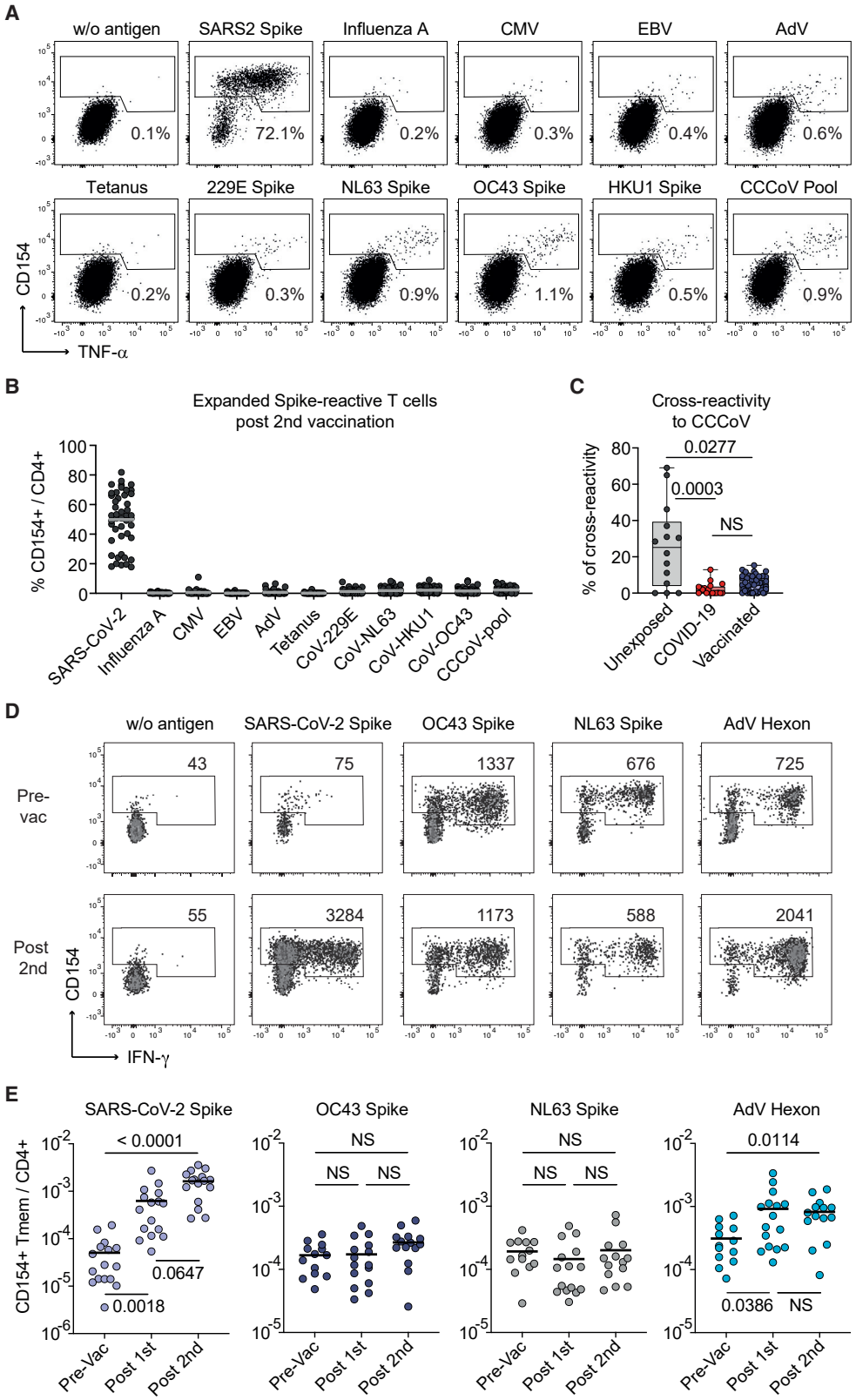

Figure 6. CCCoV cross-reactive T cells barely contribute to the SARS-CoV-2 vaccine response

(A–C) SARS-CoV-2 spike-reactive CD154^{+} Tmems were expanded post-second vaccination and restimulated in presence of autologous antigen-presenting cells with different antigens, including individual spike proteins from CCCoVs or a pool thereof.

(legend continued on next page)

between individuals (Figures 5D and 5E). In summary, these data show that all age groups are similarly affected by the loss of reactivity against the Omicron variant. Larger cohorts are needed to clarify in the future whether the decline of reactivity against variants has stronger consequences in donors with low T cell response quality.

CCCoV cross-reactive T cells are not major contributors to the anti-SARS-CoV-2 vaccine response

Our data suggest that pre-existing memory does not strongly contribute to a high-quality vaccination response. However, pre-existing memory induced by related CCCoVs has been suggested to contribute to SARS-CoV-2 immunity upon infection and vaccination. To specifically determine the contribution of CCCoV-cross-reactive T cells to the SARS-CoV-2 spike-specific T cell response, we expanded SARS-CoV-2 spike-specific cells after the second vaccination. Restimulation proved high reactivity against the SARS-CoV-2 spike protein, but only low cross-reactivity to spike proteins from the CCCoV strains 229E, NL63, OC43, and HKU1, which was similar to other common viral antigens in individual donors (Figures 6A and 6B). Based on the reactivity to SARS-CoV-2 spike proteins and a pool of all four CCCoV spike proteins, we calculated the percentage of cross-reactivity for each donor. This revealed on average 5% cross-reactivity of the SARS-CoV-2 spike-specific T cells against CCCoVs upon vaccination, which was in a similar magnitude, as observed before, in COVID-19 patients (Figure 6C; Bacher et al., 2020).

Conversely, we analyzed whether vaccination affects the frequencies of T cells reactive against the spike proteins of CCCoVs, specifically the alpha coronavirus NL63 and the beta coronavirus OC43. As a high control for a cross-reactive response, we included the human adenovirus 5 hexon protein and restricted our analysis to the vaccinees receiving the first immunization with the adenovirus-vector-based ChAdOx1 vaccine, followed by Moderna mRNA-1273 (Figure 1A). Sequence alignment of the hexon protein from chimpanzee adenovirus Y25, which was used as a vector for ChAdOx1, showed high sequence homology (80% identity) with the human AdV5 hexon, whereas SARS-CoV-2 and CCCoV spike proteins had 30% sequence identity (Figure S6). Despite a 1–2 log increase of SARS-CoV-2 spike-specific T cells, CCCoV spike-reactive T cell frequencies remained stable post-vaccination (Figures 6D and 6E). In contrast, the response to the adenovirus hexon protein was increased after ChAdOx1 vaccination and remained stable afterward (Figures 6D and 6E). This indicates that cross-reactive T cells are increased upon vaccination when sequence homology is high enough, as it is the case for adenovirus hexon-specific cells.

In summary, these data further indicate that CCCoV cross-reactive T cells are not the major drivers of the SARS-CoV-2 spike-specific $CD4^+$ T cells upon vaccination, as previously also shown for SARS-CoV-2 infection (Bacher et al., 2020; Low et al., 2021; Mateus et al., 2020).

DISCUSSION

High immune-response variability is a critical feature of SARS-CoV-2 infection and vaccination. Understanding the individual intrinsic parameters determining the immune-response quality is key to identifying high-risk subgroups and developing protective measures. So far, it is poorly understood as to how the antigen-specific pre-exposure T cell repertoire impacts immune-response quality and how this is affected by age as the most relevant risk factor for poor protection. Our data showed that the response to SARS-CoV-2 vaccination is determined by the pre-exposure T cell repertoire, comprising two separate entities with opposing effects: SARS-CoV-2-specific naive and pre-existing memory T cells. Both are inversely affected by aging and together identify individuals at risk for impaired immunity.

Technical limitations in tracking rare antigen-specific T cells in unexposed individuals have restricted the study of the effect of the pre-vaccination repertoire on the immune-response quality. Rare cell-enrichment approaches allow identification of naive and memory T cells in the pre-exposure repertoire (Bacher et al., 2013, 2016, 2019, 2020; Moon et al., 2007; Obar et al., 2008; Pan et al., 2021; Su et al., 2013). Without enrichment, the detection is mainly restricted to high-frequency memory T cells and only in a variable fraction of unexposed donors (Bacher and Scheffold, 2013; Braun et al., 2020; Grifoni et al., 2020; Loyal et al., 2021; Mateus et al., 2021; Ogbe et al., 2021). By using ARTE, we identified the antigen-specific $CD4^+$ T cell expansion rate as a critical parameter for vaccine-response quality, which was directly linked to the pre-vaccination repertoire. Rare T cell precursors with high expansion potential, likely from the naive repertoire, supported strong expansion upon vaccination, whereas pre-existing memory cells counteracted it.

Our data identified two interdependent, but not directly linked, parameters affecting immune-response quality: first, in the elderly, $CD4^+$ T cell expansion of both the naive and memory compartment was severely compromised. This is in line with the current concept that aging has a strong effect on the T cell repertoire, with a decline in naive T cells and an impaired memory compartment (Mittelbrunn and Kroemer, 2021), which we confirmed here for SARS-CoV-2-specific T cells. Second, similar repertoire restrictions also occurred in individuals from younger

(A) Representative dot plots for re-stimulation. Percentage of $CD154^+TNF\alpha^+$ cells within $CD4^+$ is indicated.
(B) Summarized reactivity of the expanded cell lines against different antigens (n = 46).
(C) Percentage of cross-reactivity of SARS-CoV-2 spike-reactive cells to the pool of CCCoV spike proteins in unexposed donors (n = 14), COVID-19 patients (n = 18), and SARS-CoV-2 vaccinees (n = 46).
(D and E) $CD4^+$ T cells specific for SARS-CoV-2 spike, OC43 spike, NL63 spike, and AdV hexon were analyzed in 16 individuals receiving a heterologous vaccination with the adenovirus-vector-based ChAdOx1 vaccine, followed by Moderna mRNA-1273.
(D) Representative dot plot examples for *ex vivo* detection of antigen-reactive $CD4^+$ T cells by ARTE pre- and post-vaccination. Absolute cell counts after magnetic $CD154^+$ enrichment from 1x10e7 PBMCs are indicated.
(E) Frequencies of Tmems reactive for the indicated antigens pre- and post-SARS-CoV-2 vaccination (n = 16). Each symbol in (B, C, E) represents one donor; horizontal lines indicate mean in (B, E). Box-and-whisker plots display quartiles and range in (C). Statistical differences: Kruskal-Wallis test with Dunn's post hoc test in (C, E). See also Figure S6.

age groups with a high contribution of pre-existing memory cells, suggesting that this is a general parameter determining immune-response quality to SARS-CoV-2.

While the importance of the naive compartment is well accepted, the *in vivo* contribution of pre-existing memory cells is not clear (Lipsitch et al., 2020; Moss, 2022; Woodland and Blackman, 2006). Pre-existing memory T cells have been described for SARS-CoV-2 (Bacher et al., 2020; Bartolo et al., 2021; Braun et al., 2020; Le Bert et al., 2020; Loyal et al., 2021; Mateus et al., 2020; Nelde et al., 2020), but also for many other pathogens (Bacher et al., 2013; Campion et al., 2014; Kwok et al., 2012; Pan et al., 2021; Su et al., 2013). Conflicting data exists regarding the age-associated prevalence of SARS-CoV-2-reactive pre-existing memory T cells (Bacher et al., 2020; Dowell et al., 2022; Loyal et al., 2021; Saletti et al., 2020). Recent correlative data suggested that pre-existing memory T cells may support an earlier and stronger anti-SARS-CoV-2 T and B cell reaction following infection or vaccination (Kundu et al., 2022; Loyal et al., 2021; Mateus et al., 2021; Meyer-Arndt et al., 2022; Swadling et al., 2022). A limitation of these studies is that they are based on technologies that only incompletely resolve the pre-vaccination repertoire, and the contribution of individual clonotypes to the *in vivo* response was not analyzed. By using clonal TCR tracking, we revealed a minimal contribution of pre-existing memory T cells in most individuals, which correlated with high T cell expansion. This indicates that in high-quality responders, pre-existing memory clones are surpassed by multiple strongly expanding low-frequency precursors, most likely from the naive pool. A similar clonal hierarchy shift was recently demonstrated for yellow fever vaccination (Pan et al., 2021). In contrast, individuals where pre-existing memory clonotypes remained dominant after vaccination displayed rather poor responses and a lower TCR diversity, as previously shown in mice (Cornberg et al., 2006). Low-avidity pre-existing memory cells may prevent naive T cell recruitment and high-affinity selection (Lanzer et al., 2014). Overall, this emphasizes the central importance of strong clonal expansions of diverse and high-avidity precursors that together form a high-quality T cell response.

A diverse TCR repertoire, rather than T cell abundance, was shown to be protective in pathogen-specific immunity (Wang et al., 2012). Furthermore, a limited TCR diversity has been associated with escape of viral mutants (Cornberg et al., 2006; Meyer-Olson et al., 2004). However, with our small number of analyzed individuals, we did not observe a particular reduction of the $CD4^+$ T cell response to the B.1.1.529 Omicron variant in the elderly or in younger donors with low TCR diversity due to a high contribution of pre-existing memory. Instead, the decline against the Omicron variant was highly variable between the donors. This suggests that additional parameters such as precise epitope specificities or human leukocyte antigen (HLA) alleles might be important for successful adaption to viral variants. Nevertheless, given the already low frequencies and quality of spike-specific T cells in individual donors and especially the >80 years group, a further reduction by viral variants such as Omicron suggests a remaining vulnerability of these individuals despite vaccination. Clearly, larger cohorts are needed to address this point in more depth.

A protective role of pre-existing memory T cells has initially been proposed due to cross-reactivity to related CCCoVs. However, CCCoV-reactive T cells only account for a variable part of the pre-existing memory to SARS-CoV-2 (Bacher et al., 2020; Bartolo et al., 2021). CCCoV cross-reactivity was reduced following vaccination, as previously demonstrated for SARS-CoV-2 infection (Bacher et al., 2020; Mateus et al., 2020), most likely due to low avidity of cross-reactive TCRs (Bacher et al., 2020; Dykema et al., 2021). In contrast, we found strong expansion of adenovirus hexon-specific memory T cells by the adenovector-based AstraZeneca ChAdOx1 vaccine. Similarly, clonal tracking after influenza vaccination shows strong involvement of memory T cells (Hill et al., 2021; Nienen et al., 2019). Thus, the role of pre-existing T cell memory is context dependent: effective cross-reactive T cell memory activation *in vivo* appears to depend on high affinity to homologous peptides, which seems to apply only to a minority of SARS-CoV-2 epitopes. Whether such rare pre-existing TCRs can directly contribute to an earlier response to SARS-CoV-2 in individual donors (Loyal et al., 2021; Mateus et al., 2021) remains to be further investigated.

High age is also a risk factor for severe COVID-19. SARS-CoV-2-specific $CD4^+$ T cell frequencies are increased in severe COVID-19 (Moss, 2022), whereas decreased frequencies are found in old vaccinees (Anderson et al., 2020; Collier et al., 2021; Li et al., 2021; Romero-Olmedo et al., 2022a). However, in both situations, we identified similar low-avidity T cell responses (Bacher et al., 2020). This suggests that the recruitment of low-avidity T cells, presumably from an impaired pre-exposure repertoire, is a common denominator of low-quality T cell responses. A higher dose, dissemination, and persistence of viral antigen or stronger costimulatory signals may account for the increased frequency of low-avidity SARS-CoV-2-specific T cells in severe COVID-19, as compared to vaccination.

In summary, a compromised pre-exposure repertoire determined low-quality $CD4^+$ T cell responses, which is the common feature of poor vaccine responses, as well as severe COVID-19. Importantly, such a T cell repertoire-intrinsic defect may not be rescued by repeated vaccination (Romero-Olmedo et al., 2022a, 2022b), but vice versa: a low-quality T cell response to vaccination may explain why the elderly remain at higher risk for developing severe disease (Yek et al., 2022). Thus, our results highlight the need to develop novel vaccination strategies targeting or diversifying restricted T cell repertoires in individuals at risk.

Limitations of the study

Our study is restricted to only a small number of individuals within the different age groups due to the high experimental effort required for antigen-specific T cell enrichment and clonal tracking. Clonal tracking in the pre-immune repertoire is technically challenging and restricted to abundant precursor clones. Therefore, small precursor clones that might contribute to the post-vaccination response might be missed. Since we could not analyze the pre-vaccine naive TCR repertoire due to technical limitations in tracking low numbers of cells with low clonality, the direct origin of the rare, strongly proliferating clones in high-quality responders remains undefined, and a potential contribution of tissue-derived or stem cell memory cells cannot be excluded. Furthermore, the antigens driving the pre-existing memory response in different individuals remain unknown. Our analysis describes the average contribution of the pre-existing

memory population as well as the average of T cell quality parameters such as fold expansion and functional avidity. Individual T cell clones also may act differently in individual donors, and a positive contribution of individual pre-existing T cell clones to SARS-CoV-2 immunity remains to be further elucidated.

STAR★METHODS

Detailed methods are provided in the online version of this paper and include the following:

- KEY RESOURCES TABLE
- RESOURCE AVAILABILITY
  - Lead contact
  - Materials availability
  - Data and code availability
- EXPERIMENTAL MODEL AND SUBJECT DETAILS
  - Blood donors
  - Vero cells
- METHOD DETAILS
  - Antigens
  - Antigen-reactive T cell enrichment (ARTE)
  - Flow cytometry
  - Quantification of SARS-CoV-2 spike-specific antibodies
  - Measurement of SARS-CoV-2-neutralizing antibodies
  - Expansion and re-stimulation of antigen-reactive T cells
  - Analysis of functional avidity
  - T cell receptor (TCR) sequencing
  - TCR repertoire analyses
  - TCR similarity analyses
- QUANTIFICATION AND STATISTICAL ANALYSIS
  - Software

SUPPLEMENTAL INFORMATION

Supplemental information can be found online at https://doi.org/10.1016/j.immuni.2022.08.003.

ACKNOWLEDGMENTS

We thank Ulf Klein for critical reading of the manuscript; Anastasia Minervina and Mikhail Pogorelyy for their support with the TCRdist analysis and visualization; the flow cytometry facility, Cyto Kiel, and the Competence Centre for Genomic Analysis (CCGA) for support with cell sorting and TCR sequencing; and Monika Brüggemann, Patience Eschenhagen, Vanessa März, and Ina Martens for help with recruitment of study participants or technical assistance. This research was supported by the German Research Foundation (DFG) under Germany's Excellence Strategy - EXC 2167-390884018 Precision Medicine in Chronic Inflammation (to A.F., S.S., B.H., A.S., P.B.); RU5042 – miTarget to A.F., P.B.; DFG grant no. 433038070 (to P.B., A.F., and A.S.); and a COVID-19 research grant from the Land Schleswig-Holstein, DIO002/CoVispecT (to P.B., A.S.).

AUTHOR CONTRIBUTIONS

Conceptualization: P.B., A.S.; investigation: C.Sa., G.R.M., E.R., S.M., B.M., A.K.K., N.B., J.G., R.R., M.V., U.M.G., H.M.R., P.B.; formal analysis: P.B., E.R.; resources: M.S., F.T., D.K.B., A.K., H.F., O.K., Y.K., M.J.G.T.V., O.C., P.K., A.F., C.Sch., S.S., B.H.; visualization: P.B., E.R.; supervision: A.K., H.F., A.F., S.S., B.H., A.S., P.B.; funding acquisition: P.B., A.S.; all authors provided discussion, participated in revising the manuscript, and agreed to the final version.

DECLARATION OF INTERESTS

E.R. is employee of Evotec SE. O.K. is employee of Peptides & elephants GmbH. O.C. reports grants or contracts from MSD, Pfizer; consulting fees from Biocon, Molecular Partners, Noxxon, PSI; honoraria for lectures from Abbott, Pfizer; participation on a data safety monitoring board or advisory board from Jannsen, PSI. P.K. reports grants or contracts from BMBF, B-FAST, and NAPKON of the Network University Medicine and the State of North Rhine-Westphalia; consulting fees from Ambu GmbH, Gilead Sciences, Noxxon N.V., Pfizer Pharma; honoraria for lectures from Ambu GmbH, Gilead Sciences, MSD Sharp & Dohme GmbH, Pfizer Pharma GmbH, Scilink Comunicación Científica SC; participation on an advisory board from Ambu GmbH, Gilead Sciences, Pfizer Pharma.

Received: March 14, 2022
Revised: June 23, 2022
Accepted: August 8, 2022
Published: August 12, 2022

REFERENCES

Allen, J.C., Toapanta, F.R., Chen, W., and Tennant, S.M. (2020). Understanding immunosenescence and its impact on vaccination of older adults. Vaccine *38*, 8264–8272. https://doi.org/10.1016/j.vaccine.2020.11.002.

Anderson, E.J., Rouphael, N.G., Widge, A.T., Jackson, L.A., Roberts, P.C., Makhene, M., Chappell, J.D., Denison, M.R., Stevens, L.J., Pruijssers, A.J., et al. (2020). Safety and immunogenicity of SARS-CoV-2 mRNA-1273 vaccine in older adults. N. Engl. J. Med. *383*, 2427–2438. https://doi.org/10.1056/NEJMoa2028436.

Bacher, P., Heinrich, F., Stervbo, U., Nienen, M., Vahldieck, M., Iwert, C., Vogt, K., Kollet, J., Babel, N., Sawitzki, B., et al. (2016). Regulatory T cell specificity directs tolerance versus allergy against aeroantigens in humans. Cell *167*, 1067–1078.e16. https://doi.org/10.1016/j.cell.2016.09.050.

Bacher, P., Hohnstein, T., Beerbaum, E., Röcker, M., Blango, M.G., Kaufmann, S., Röhmel, J., Eschenhagen, P., Grehn, C., Seidel, K., et al. (2019). Human anti-fungal Th17 Immunity and pathology rely on cross-reactivity against candida albicans. Cell *176*, 1340–1355.e15. https://doi.org/10.1016/j.cell.2019.01.041.

Bacher, P., Rosati, E., Esser, D., Martini, G.R., Saggau, C., Schiminsky, E., Dargvainiene, J., Schröder, I., Wieters, I., Khodamoradi, Y., et al. (2020). Low-Avidity CD4(+) T Cell responses to SARS-CoV-2 in unexposed individuals and humans with severe COVID-19. Immunity *53*, 1258–1271.e5. https://doi.org/10.1016/j.immuni.2020.11.016.

Bacher, P., and Scheffold, A. (2013). Flow-cytometric analysis of rare antigen-specific T cells. Cytometry A. *83*, 692–701. https://doi.org/10.1002/cyto.a.22317.

Bacher, P., Schink, C., Teutschbein, J., Kniemeyer, O., Assenmacher, M., Brakhage, A.A., and Scheffold, A. (2013). Antigen-reactive T cell enrichment for direct, high-resolution analysis of the human naive and memory Th cell repertoire. J. Immunol. *190*, 3967–3976. https://doi.org/10.4049/jimmunol.1202221.

Bartolo, L., Afroz, S., Pan, Y.G., Xu, R., Williams, L., Lin, C.F., Friedman, E.S., Gimotty, P.A., Wu, G.D., and Su, L.F. (2021). SARS-CoV-2-specific T cells in unexposed adults display broad trafficking potential and cross-react with commensal antigens. Preprint at bioRxiv. https://doi.org/10.1101/2021.11.29.470421.

Bastian, M., Heymann, S., and Jacomy, M. (2009). Gephi: An Open Source Software for Exploring and Manipulating Networks. Proceedings of the International AAAI Conference on Web and Social Media *3*, 361–362.

Birnbaum, M.E., Mendoza, J.L., Sethi, D.K., Dong, S., Glanville, J., Dobbins, J., Ozkan, E., Davis, M.M., Wucherpfennig, K.W., and Garcia, K.C. (2014).

Deconstructing the peptide-MHC specificity of T cell recognition. Cell *157*, 1073–1087. https://doi.org/10.1016/j.cell.2014.03.047.

Bolotin, D.A., Poslavsky, S., Mitrophanov, I., Shugay, M., Mamedov, I.Z., Putintseva, E.V., and Chudakov, D.M. (2015). MiXCR: software for comprehensive adaptive immunity profiling. Nat. Methods *12*, 380–381. https://doi.org/10.1038/nmeth.3364.

Braun, J., Loyal, L., Frentsch, M., Wendisch, D., Georg, P., Kurth, F., Hippenstiel, S., Dingeldey, M., Kruse, B., Fauchere, F., et al. (2020). SARS-CoV-2-reactive T cells in healthy donors and patients with COVID-19. Nature *587*, 270–274. https://doi.org/10.1038/s41586-020-2598-9.

Campion, S.L., Brodie, T.M., Fischer, W., Korber, B.T., Rossetti, A., Goonetilleke, N., McMichael, A.J., and Sallusto, F. (2014). Proteome-wide analysis of HIV-specific naive and memory CD4(+) T cells in unexposed blood donors. J. Exp. Med. *211*, 1273–1280. https://doi.org/10.1084/jem.20130555.

Cicin-Sain, L., Smyk-Pearson, S., Smyk-Paerson, S., Currier, N., Byrd, L., Koudelka, C., Robinson, T., Swarbrick, G., Tackitt, S., Legasse, A., et al. (2010). Loss of naive T cells and repertoire constriction predict poor response to vaccination in old primates. J. Immunol. *184*, 6739–6745. https://doi.org/10.4049/jimmunol.0904193.

Collier, D.A., Ferreira, I.A.T.M., Kotagiri, P., Datir, R.P., Lim, E.Y., Touizer, E., Meng, B., Abdullahi, A.; CITIID-NIHR BioResource COVID-19 Collaboration, and Elmer, A., et al. (2021). Age-related immune response heterogeneity to SARS-CoV-2 vaccine BNT162b2. Nature *596*, 417–422. https://doi.org/10.1038/s41586-021-03739-1.

Cornberg, M., Chen, A.T., Wilkinson, L.A., Brehm, M.A., Kim, S.K., Calcagno, C., Ghersi, D., Puzone, R., Celada, F., Welsh, R.M., and Selin, L.K. (2006). Narrowed TCR repertoire and viral escape as a consequence of heterologous immunity. J. Clin. Invest. *116*, 1443–1456. https://doi.org/10.1172/JCI27804.

Csardi, G., and Nepusz, T. (2006). The igraph software package for complex network research. InterJournal, Complex Systems *1695*. https://igraph.org.

Dash, P., Fiore-Gartland, A.J., Hertz, T., Wang, G.C., Sharma, S., Souquette, A., Crawford, J.C., Clemens, E.B., Nguyen, T.H.O., Kedzierska, K., et al. (2017). Quantifiable predictive features define epitope-specific T cell receptor repertoires. Nature *547*, 89–93. https://doi.org/10.1038/nature22383.

Dowell, A.C., Butler, M.S., Jinks, E., Tut, G., Lancaster, T., Sylla, P., Begum, J., Bruton, R., Pearce, H., Verma, K., et al. (2022). Children develop robust and sustained cross-reactive spike-specific immune responses to SARS-CoV-2 infection. Nat. Immunol. *23*, 40–49. https://doi.org/10.1038/s41590-021-01089-8.

Dykema, A.G., Zhang, B., Woldemeskel, B.A., Garliss, C.C., Cheung, L.S., Choudhury, D., Zhang, J., Aparicio, L., Bom, S., Rashid, R., et al. (2021). Functional characterization of CD4+ T cell receptors crossreactive for SARS-CoV-2 and endemic coronaviruses. J. Clin. Invest. *131*, 146922. https://doi.org/10.1172/JCI146922.

Geisen, U.M., Berner, D.K., Tran, F., Sümbül, M., Vullriede, L., Ciripoi, M., Reid, H.M., Schaffarzyk, A., Longardt, A.C., Franzenburg, J., et al. (2021a). Immunogenicity and safety of anti-SARS-CoV-2 mRNA vaccines in patients with chronic inflammatory conditions and immunosuppressive therapy in a monocentric cohort. Ann. Rheum. Dis. *80*, 1306–1311. https://doi.org/10.1136/annrheumdis-2021-220272.

Geisen, U.M., Sümbül, M., Tran, F., Berner, D.K., Reid, H.M., Vullriede, L., Ciripoi, M., Longardt, A.C., Hoff, P., Morrison, P.J., et al. (2021b). Humoral protection to SARS-CoV2 declines faster in patients on TNF alpha blocking therapies. RMD Open *7*, e002008. https://doi.org/10.1136/rmdopen-2021-002008.

Grifoni, A., Weiskopf, D., Ramirez, S.I., Mateus, J., Dan, J.M., Moderbacher, C.R., Rawlings, S.A., Sutherland, A., Premkumar, L., Jadi, R.S., et al. (2020). Targets of T Cell Responses to SARS-CoV-2 Coronavirus in Humans with COVID-19 Disease and Unexposed Individuals. Cell *181*, 1489–1501.e15. https://doi.org/10.1016/j.cell.2020.05.015.

Guerrera, G., Picozza, M., D'Orso, S., Placido, R., Pirronello, M., Verdiani, A., Termine, A., Fabrizio, C., Giannessi, F., Sambucci, M., et al. (2021). BNT162b2 vaccination induces durable SARS-CoV-2-specific T cells with a stem cell memory phenotype. Sci. Immunol. *6*, eabl5344. https://doi.org/10.1126/sciimmunol.abl5344.

Gustafson, C.E., Kim, C., Weyand, C.M., and Goronzy, J.J. (2020). Influence of immune aging on vaccine responses. J. Allergy Clin. Immunol. *145*, 1309–1321. https://doi.org/10.1016/j.jaci.2020.03.017.

Hill, D.L., Whyte, C.E., Innocentin, S., Lee, J.L., Dooley, J., Wang, J., James, E.A., Lee, J.C., Kwok, W.W., Zand, M.S., et al. (2021). Impaired HA-specific T follicular helper cell and antibody responses to influenza vaccination are linked to inflammation in humans. Elife *10*, e70554. https://doi.org/10.7554/eLife.70554.

Juthani, P.V., Gupta, A., Borges, K.A., Price, C.C., Lee, A.I., Won, C.H., and Chun, H.J. (2021). Hospitalisation among vaccine breakthrough COVID-19 infections. Lancet Infect. Dis. *21*, 1485–1486. https://doi.org/10.1016/S1473-3099(21)00558-2.

Kundu, R., Narean, J.S., Wang, L., Fenn, J., Pillay, T., Fernandez, N.D., Conibear, E., Koycheva, A., Davies, M., Tolosa-Wright, M., et al. (2022). Cross-reactive memory T cells associate with protection against SARS-CoV-2 infection in COVID-19 contacts. Nat. Commun. *13*, 80. https://doi.org/10.1038/s41467-021-27674-x.

Kwok, W.W., Tan, V., Gillette, L., Littell, C.T., Soltis, M.A., LaFond, R.B., Yang, J., James, E.A., and DeLong, J.H. (2012). Frequency of epitope-specific naive CD4(+) T cells correlates with immunodominance in the human memory repertoire. J. Immunol. *188*, 2537–2544. https://doi.org/10.4049/jimmunol.1102190.

Lanzer, K.G., Johnson, L.L., Woodland, D.L., and Blackman, M.A. (2014). Impact of ageing on the response and repertoire of influenza virus-specific CD4 T cells. Immun. Ageing *11*, 9. https://doi.org/10.1186/1742-4933-11-9.

Le Bert, N., Tan, A.T., Kunasegaran, K., Tham, C.Y.L., Hafezi, M., Chia, A., Chng, M.H.Y., Lin, M., Tan, N., Linster, M., et al. (2020). SARS-CoV-2-specific T cell immunity in cases of COVID-19 and SARS, and uninfected controls. Nature *584*, 457–462. https://doi.org/10.1038/s41586-020-2550-z.

Li, J., Hui, A., Zhang, X., Yang, Y., Tang, R., Ye, H., Ji, R., Lin, M., Zhu, Z., Türeci, Ö., et al. (2021). Safety and immunogenicity of the SARS-CoV-2 BNT162b1 mRNA vaccine in younger and older Chinese adults: a randomized, placebo-controlled, double-blind phase 1 study. Nat. Med. *27*, 1062–1070. https://doi.org/10.1038/s41591-021-01330-9.

Lipsitch, M., Grad, Y.H., Sette, A., and Crotty, S. (2020). Cross-reactive memory T cells and herd immunity to SARS-CoV-2. Nat. Rev. Immunol. *20*, 709–713. https://doi.org/10.1038/s41577-020-00460-4.

Low, J.S., Vaqueirinho, D., Mele, F., Foglierini, M., Jerak, J., Perotti, M., Jarrossay, D., Jovic, S., Perez, L., Cacciatore, R., et al. (2021). Clonal analysis of immunodominance and cross-reactivity of the CD4 T cell response to SARS-CoV-2. Science *372*, 1336–1341. https://doi.org/10.1126/science.abg8985.

Loyal, L., Braun, J., Henze, L., Kruse, B., Dingeldey, M., Reimer, U., Kern, F., Schwarz, T., Mangold, M., Unger, C., et al. (2021). Cross-reactive CD4(+) T cells enhance SARS-CoV-2 immune responses upon infection and vaccination. Science *374*, eabh1823. https://doi.org/10.1126/science.abh1823.

Mallajosyula, V., Ganjavi, C., Chakraborty, S., McSween, A.M., Pavlovitch-Bedzyk, A.J., Wilhelmy, J., Nau, A., Manohar, M., Nadeau, K.C., and Davis, M.M. (2021). CD8(+) T cells specific for conserved coronavirus epitopes correlate with milder disease in COVID-19 patients. Sci. Immunol. *6*, eabg5669. https://doi.org/10.1126/sciimmunol.abg5669.

Mateus, J., Dan, J.M., Zhang, Z., Rydyznski Moderbacher, C., Lammers, M., Goodwin, B., Sette, A., Crotty, S., and Weiskopf, D. (2021). Low-dose mRNA-1273 COVID-19 vaccine generates durable memory enhanced by cross-reactive T cells. Science *374*, eabj9853. https://doi.org/10.1126/science.abj9853.

Mateus, J., Grifoni, A., Tarke, A., Sidney, J., Ramirez, S.I., Dan, J.M., Burger, Z.C., Rawlings, S.A., Smith, D.M., Phillips, E., et al. (2020). Selective and cross-reactive SARS-CoV-2 T cell epitopes in unexposed humans. Science *370*, 89–94. https://doi.org/10.1126/science.abd3871.

Meyer-Arndt, L., Schwarz, T., Loyal, L., Henze, L., Kruse, B., Dingeldey, M., Gürcan, K., Uyar-Aydin, Z., Müller, M.A., Drosten, C., et al. (2022). Cutting edge: serum but not mucosal antibody responses are associated with pre-existing SARS-CoV-2 Spike Cross-Reactive CD4(+) T Cells following BNT162b2

vaccination in the elderly. J. Immunol. *208*, 1001–1005. https://doi.org/10.4049/jimmunol.2100990.

Meyer-Olson, D., Shoukry, N.H., Brady, K.W., Kim, H., Olson, D.P., Hartman, K., Shintani, A.K., Walker, C.M., and Kalams, S.A. (2004). Limited T cell receptor diversity of HCV-specific T cell responses is associated with CTL escape. J. Exp. Med. *200*, 307–319. https://doi.org/10.1084/jem.20040638.

Mittelbrunn, M., and Kroemer, G. (2021). Hallmarks of T cell aging. Nat. Immunol. *22*, 687–698. https://doi.org/10.1038/s41590-021-00927-z.

Moon, J.J., Chu, H.H., Pepper, M., McSorley, S.J., Jameson, S.C., Kedl, R.M., and Jenkins, M.K. (2007). Naive CD4(+) T cell frequency varies for different epitopes and predicts repertoire diversity and response magnitude. Immunity *27*, 203–213. https://doi.org/10.1016/j.immuni.2007.07.007.

Moss, P. (2022). The T cell immune response against SARS-CoV-2. Nat. Immunol. *23*, 186–193. https://doi.org/10.1038/s41590-021-01122-w.

Mudd, P.A., Minervina, A.A., Pogorelyy, M.V., Turner, J.S., Kim, W., Kalaidina, E., Petersen, J., Schmitz, A.J., Lei, T., Haile, A., et al. (2022). SARS-CoV-2 mRNA vaccination elicits a robust and persistent T follicular helper cell response in humans. Cell *185*, 603–613.e15. https://doi.org/10.1016/j.cell.2021.12.026.

Nelde, A., Bilich, T., Heitmann, J.S., Maringer, Y., Salih, H.R., Roerden, M., Lübke, M., Bauer, J., Rieth, J., Wacker, M., et al. (2021). SARS-CoV-2-derived peptides define heterologous and COVID-19-induced T cell recognition. Nat. Immunol. *22*, 74–85. https://doi.org/10.1038/s41590-020-00808-x.

Neumann, F., Rose, R., Rompke, J., Grobe, O., Lorentz, T., Fickenscher, H., and Krumbholz, A. (2021). Development of SARS-CoV-2 Specific IgG and Virus-Neutralizing Antibodies after Infection with Variants of Concern or Vaccination. Vaccines (Basel) *9*, 700. https://doi.org/10.3390/vaccines9070700.

Nienen, M., Stervbo, U., Mölder, F., Kaliszczyk, S., Kuchenbecker, L., Gayova, L., Schweiger, B., Jürchott, K., Hecht, J., Neumann, A.U., et al. (2019). The Role of Pre-existing Cross-Reactive Central Memory CD4 T-Cells in Vaccination With Previously Unseen Influenza Strains. Front. Immunol. *10*, 593. https://doi.org/10.3389/fimmu.2019.00593.

Obar, J.J., Khanna, K.M., and Lefrançois, L. (2008). Endogenous naive CD8+ T cell precursor frequency regulates primary and memory responses to infection. Immunity *28*, 859–869. https://doi.org/10.1016/j.immuni.2008.04.010.

Ogbe, A., Kronsteiner, B., Skelly, D.T., Pace, M., Brown, A., Adland, E., Adair, K., Akhter, H.D., Ali, M., Ali, S.E., et al. (2021). T cell assays differentiate clinical and subclinical SARS-CoV-2 infections from cross-reactive antiviral responses. Nat. Commun. *12*, 2055. https://doi.org/10.1038/s41467-021-21856-3.

Oksanen, J.B., F., G., Friendly, M., Kindt, R., Legendre, P., McGlinn, D., Minchin, P.R., O'Hara, R.B., Simpson, G.L., Solymos, P., Stevens, M.H.H., et al. (2019). vegan: community ecology package. R package version 2.5-6. https://CRAN.R-project.org/package=vegan.

Pan, Y.G., Aiamkitsumrit, B., Bartolo, L., Wang, Y., Lavery, C., Marc, A., Holec, P.V., Rappazzo, C.G., Eilola, T., Gimotty, P.A., et al. (2021). Vaccination reshapes the virus-specific T cell repertoire in unexposed adults. Immunity *54*, 1245–1256.e5. https://doi.org/10.1016/j.immuni.2021.04.023.

Rényi, A. (1961). On measures of information and entropy. Proc. 4th Berkley Symp. Math. Stat. Prob. *1*, 547–561.

Romero-Olmedo, A.J., Schulz, A.R., Hochstätter, S., Das Gupta, D., Virta, I., Hirseland, H., Staudenraus, D., Camara, B., Münch, C., Hefter, V., et al. (2022a). Induction of robust cellular and humoral immunity against SARS-CoV-2 after a third dose of BNT162b2 vaccine in previously unresponsive older adults. Nat. Microbiol. *7*, 195–199. https://doi.org/10.1038/s41564-021-01046-z.

Romero-Olmedo, A.J., Schulz, A.R., Hochstätter, S., Gupta, D.D., Hirseland, H., Staudenraus, D., Camara, B., Volland, K., Hefter, V., Sapre, S., et al. (2022b). Dynamics of humoral and T-cell immunity after three BNT162b2 vaccinations in adults older than 80 years. Lancet Infect. Dis. *22*, 588–589. https://doi.org/10.1016/S1473-3099(22)00219-5.

Rosati, E., Pogorelyy, M.V., Minervina, A.A., Scheffold, A., Franke, A., Bacher, P., and Thomas, P.G. (2021). Characterization of SARS-CoV-2 public CD4+ alphabeta T cell clonotypes through reverse epitope discovery. Preprint at bioRxiv. https://doi.org/10.1101/2021.11.19.469229.

Rose, R., Neumann, F., Grobe, O., Lorentz, T., Fickenscher, H., and Krumbholz, A. (2022a). Humoral immune response after different SARS-CoV-2 vaccination regimens. BMC Med. *20*, 31. https://doi.org/10.1186/s12916-021-02231-x.

Rose, R., Neumann, F., Müller, S., Bäumler, C., Schäfer, M., Schön, F., Römpke, J., Schulze, S., Weyer, D., Grobe, O., et al. (2022b). Delta or Omicron BA.1/2-neutralizing antibody levels and T-cell reactivity after triple-vaccination or infection. Allergy. https://doi.org/10.1111/all.15395.

Saletti, G., Gerlach, T., Jansen, J.M., Molle, A., Elbahesh, H., Ludlow, M., Li, W., Bosch, B.J., Osterhaus, A.D.M.E., and Rimmelzwaan, G.F. (2020). Older adults lack SARS CoV-2 cross-reactive T lymphocytes directed to human coronaviruses OC43 and NL63. Sci. Rep. *10*, 21447. https://doi.org/10.1038/s41598-020-78506-9.

Schattgen, S.A., Guion, K., Crawford, J.C., Souquette, A., Barrio, A.M., Stubbington, M.J.T., Thomas, P.G., and Bradley, P. (2022). Integrating T cell receptor sequences and transcriptional profiles by clonotype neighbor graph analysis (CoNGA). Nat. Biotechnol. *40*, 54–63. https://doi.org/10.1038/s41587-021-00989-2.

Sewell, A.K. (2012). Why must T cells be cross-reactive? Nat. Rev. Immunol. *12*, 669–677. https://doi.org/10.1038/nri3279.

Shugay, M., Britanova, O.V., Merzlyak, E.M., Turchaninova, M.A., Mamedov, I.Z., Tuganbaev, T.R., Bolotin, D.A., Staroverov, D.B., Putintseva, E.V., Plevova, K., et al. (2014). Towards error-free profiling of immune repertoires. Nat. Methods *11*, 653–655. https://doi.org/10.1038/nmeth.2960.

Stervbo, U., Rahmann, S., Roch, T., Westhoff, T.H., and Babel, N. (2020). Epitope similarity cannot explain the pre-formed T cell immunity towards structural SARS-CoV-2 proteins. Sci. Rep. *10*, 18995. https://doi.org/10.1038/s41598-020-75972-z.

Strömer, A., Rose, R., Grobe, O., Neumann, F., Fickenscher, H., Lorentz, T., and Krumbholz, A. (2020a). Kinetics of Nucleo- and Spike Protein-Specific Immunoglobulin G and of Virus-Neutralizing Antibodies after SARS-CoV-2 Infection. Microorganisms *8*, E1572. https://doi.org/10.3390/microorganisms8101572.

Strömer, A., Rose, R., Schäfer, M., Schön, F., Vollersen, A., Lorentz, T., Fickenscher, H., and Krumbholz, A. (2020b). Performance of a Point-of-Care Test for the Rapid Detection of SARS-CoV-2 Antigen. Microorganisms *9*, E58. https://doi.org/10.3390/microorganisms9010058.

Sturn, A., Quackenbush, J., and Trajanoski, Z. (2002). Genesis: cluster analysis of microarray data. Bioinformatics *18*, 207–208.

Su, L.F., Kidd, B.A., Han, A., Kotzin, J.J., and Davis, M.M. (2013). Virus-specific CD4(+) memory-phenotype T cells are abundant in unexposed adults. Immunity *38*, 373–383. https://doi.org/10.1016/j.immuni.2012.10.021.

Swadling, L., Diniz, M.O., Schmidt, N.M., Amin, O.E., Chandran, A., Shaw, E., Pade, C., Gibbons, J.M., Le Bert, N., Tan, A.T., et al. (2022). Pre-existing polymerase-specific T cells expand in abortive seronegative SARS-CoV-2. Nature *601*, 110–117. https://doi.org/10.1038/s41586-021-04186-8.

Tan, C.C.S., Owen, C.J., Tham, C.Y.L., Bertoletti, A., van Dorp, L., and Balloux, F. (2021). Pre-existing T cell-mediated cross-reactivity to SARS-CoV-2 cannot solely be explained by prior exposure to endemic human coronaviruses. Infect. Genet. Evol. *95*, 105075. https://doi.org/10.1016/j.meegid.2021.105075.

Wang, G.C., Dash, P., McCullers, J.A., Doherty, P.C., and Thomas, P.G. (2012). T cell receptor alphabeta diversity inversely correlates with pathogen-specific antibody levels in human cytomegalovirus infection. Sci. Transl. Med. *4*, 128ra42. https://doi.org/10.1126/scitranslmed.3003647.

Wang, S.Y., Juthani, P.V., Borges, K.A., Shallow, M.K., Gupta, A., Price, C., Won, C.H., and Chun, H.J. (2022). Severe breakthrough COVID-19 cases in the SARS-CoV-2 delta (B.1.617.2) variant era. Lancet. Microbe *3*, e4–e5. https://doi.org/10.1016/S2666-5247(21)00306-2.

Wickham, H. (2016). ggplot2: Elegant Graphics for Data Analysis (New York: Springer-Verlag).

Woodland, D.L., and Blackman, M.A. (2006). Immunity and age: living in the past? Trends Immunol. *27*, 303–307. https://doi.org/10.1016/j.it.2006.05.002.

Yager, E.J., Ahmed, M., Lanzer, K., Randall, T.D., Woodland, D.L., and Blackman, M.A. (2008). Age-associated decline in T cell repertoire diversity leads to holes in the repertoire and impaired immunity to influenza virus. J. Exp. Med. *205*, 711–723. https://doi.org/10.1084/jem.20071140.

Yek, C., Warner, S., Wiltz, J.L., Sun, J., Adjei, S., Mancera, A., Silk, B.J., Gundlapalli, A.V., Harris, A.M., Boehmer, T.K., and Kadri, S.S. (2022). Risk factors for severe COVID-19 outcomes among persons aged >/=18 years who completed a primary COVID-19 vaccination series - 465 Health Care Facilities, United States, December 2020-October 2021. MMWR Morb. Mortal. Wkly. Rep. *71*, 19–25. https://doi.org/10.15585/mmwr.mm7101a4.

Zeileis, A. (2014). ineq: measuring inequality, concentration, and poverty. R package version 0.2-13. https://CRAN.R-project.org/package=ineq.

STAR★METHODS

KEY RESOURCES TABLE

REAGENT or RESOURCE	SOURCE	IDENTIFIER
Antibodies		
CD4-APC-Vio770 (clone: M-T466)	Miltenyi Biotec	Cat#130-113-251 RRID:AB_2726053
CD8-VioGreen (clone: REA734)	Miltenyi Biotec	Cat#130-110-684, RRID:AB_2659241
CD14-VioGreen (clone: REA599)	Miltenyi Biotec	Cat#130-110-525 RRID:AB_2655057
CD20-VioGreen (clone: LT20)	Miltenyi Biotec	Cat#130-096-904 RRID:AB_2726147
CD38-PE-Vio770 (clone: REA572)	Miltenyi Biotec	Cat#130-113-432 RRID:AB_2733228
CD45RA-PE-Cy5 (clone: HI100)	BioLegend	Cat#304110 RRID:AB_314414
CCR7-Brilliant Violet 785 (clone: G043H7)	BioLegend	Cat#353230 RRID:AB_2563630
CD154-FITC (clone: REA238)	Miltenyi Biotec	Cat#130-109-469 RRID:AB_2751146
IL-21-PE (clone: REA1039)	Miltenyi Biotec	Cat#130-117-421, RRID:AB_2727941
TNFa-Brilliant Violet 650 (clone: MAb11)	BioLegend	Cat#502938 RRID:AB_2562741
IL-10-PE-Dazzle (clone: JES3-9D7)	BioLegend	Cat#501426 RRID:AB_2566744
IFN-γ-PerCP-Cy5.5 (clone: 4S.B3)	BioLegend	Cat#502526 RRID:AB_961355
Ki-67 Alexa Fluor 700 (clone: B56)	BD Biosciences	Cat#561277 RRID:AB_10611571
IL-2-BV711 (clone: 5344.111)	BD Biosciences	Cat#563946 RRID:AB_2738501
CD31-APC-Vio770 (clone: REA730)	Miltenyi Biotec	Cat#130-110-810 RRID:AB_2657290
CD69-PE (clone: REA824)	Miltenyi Biotec	Cat#130-112-613 RRID:AB_2659065
CD4-VioBlue (clone: VIT4)	Miltenyi Biotec	Cat#130-113-219 RRID:AB_2726030
CD154-APC (clone: 5C8)	Miltenyi Biotec	Cat#130-113-603, RRID: AB_2726191
TNF-α-PE-Vio770 (clone: cA2)	Miltenyi Biotec	Cat#130-096-755 RRID:AB_2784483
CD4-BV421 (clone: OKT4)	BioLegend	Cat#317434 RRID:AB_2562134
CD154 MicroBead Kit, human	Miltenyi Biotec	Cat#130-092-658
CD28 pure – functional grade, human (clone: 15E8)	Miltenyi Biotec	Cat#130-093-375 RRID:AB_1036134
CD40 pure – functional grade, human (clone: HB14)	Miltenyi Biotec	Cat#130-094-133 RRID:AB_10839704
CD14 MicroBeads, human	Miltenyi Biotec	Cat#130-050-201 RRID:AB_2665482
Biological samples		
Fresh human EDTA blood samples	N/A	N/A

(*Continued on next page*)

Continued

REAGENT or RESOURCE	SOURCE	IDENTIFIER
Chemicals, peptides, and recombinant proteins		
Human AB Serum	Sigma Aldrich	Cat#H4522
RPMI-1640 medium	Gibco, Life Technologies	Cat#61870-044
TexMACS medium	Miltenyi Biotec	Cat#130-097-196
X-Vivo15 medium	Lonza	Cat#BE02-060F
Human IL-2 (Proleukin)	Novartis	N/A
Human IL-4	Miltenyi Biotec	Cat#130-093-922
Human GM-CSF	Miltenyi Biotec	Cat#130-093-866
Brefeldin A	Sigma Aldrich	Cat#B7651
Critical commercial assays		
MS Columns	Miltenyi Biotec	Cat#130-042-201
LS Columns	Miltenyi Biotec	Cat#130-042-401
Viobility 405/520 Fixable Dye	Miltenyi Biotec	Cat#130-110-206
Inside Stain Kit	Miltenyi Biotec	Cat#130-090-477
RNeasy Micro Kit	Qiagen	Cat#74004
Human TCR Profiling Kit	MiLaboratory	Cat#TH-034-564252
SMARTScribe Reverse Transcriptase	Clontech	Cat#639538
RNasin Ribonuclease Inhibitor	Promega	Cat#N2511
Uracil-DNA Glycosylase	New England Biolabs	Cat#M0280S
Q5 Hot Start High-Fidelity DNA Polymerase	New England Biolabs	Cat#M0493L
Anti-Spike IgG SARS-CoV-2-QuantiVac ELISA	Euroimmun	Cat#EI 2606-9601-10 G
SARS-CoV-2 NP IgG	AESKULISA	Cat#6122
SARS-CoV-2 Neutralizing Ab ELISA Kit	Invitrogen	Cat#BMS2326
Experimental models: Cell lines		
Vero cells	CLS Cell Lines Service GmbH	Cat#605372
Software and algorithms		
FlowJo	Treestar	https://www.flowjo.com/
GraphPad Prism 9.3.1.	GraphPad	https://www.graphpad.com/
Genesis	(Sturn et al., 2002)	http://genome.tugraz.at/genesisclient/genesisclient_license.shtml
MiGEC MiGEC version 1.2.6	(Shugay et al., 2014)	N/A
MiXCR version 3.0.14	(Bolotin et al., 2015)	N/A
R package “vegan”	(Oksanen et al., 2019)	N/A
R packages “ineq”	(Zeileis, 2014)	N/A
Ggplot2	(Wickham, 2016)	N/A
Other		
PepMix™ SARS-CoV-2 (Spike Glycoprotein)	JPT	Cat#PM-WCPV-S
SARS-CoV-2 B.1.1.529 BA.1 omicron peptides	Peptides& Elephants	Cat#LB01999
SARS-CoV-2 wildtype peptides	Peptides& Elephants	Cat#LB02004
PepMix™ HCoV- HKU1 (Spike Glycoprotein)	JPT	Cat#PM-HKU1-S-1
PepMix™ HCoV-NL63 (Spike Glycoprotein)	JPT	Cat#PM-NL63-S-1
PepMix™ HCoV-OC43 (Spike Glycoprotein)	JPT	Cat# PM-OC43-S-1
PepMix™ HCoV-229E (Spike Glycoprotein)	JPT	Cat# PM-229E-S-1
PepTivator CMV pp65	Miltenyi Biotec	Cat#130-093-438
PepTivator CMV IE-1	Miltenyi Biotec	Cat#130-093-493
PepTivator Influenza A (H1N1) NA	Miltenyi Biotec	Cat#130-099-806
PepTivator Influenza A (H1N1) MP1	Miltenyi Biotec	Cat#130-097-285

(*Continued on next page*)

Continued

REAGENT or RESOURCE	SOURCE	IDENTIFIER
PepTivator Influenza A (H1N1) MP2	Miltenyi Biotec	Cat#130-099-812
PepTivator Influenza A (H1N1) NP	Miltenyi Biotec	Cat#130-097-278
PepTivator Influenza A (H1N1) HA	Miltenyi Biotec	Cat#130-099-803
PepTivator EBV BZLF1	Miltenyi Biotec	Cat#130-093-611
PepTivator EBV LMP1	Miltenyi Biotec	Cat#130-095-931
PepTivator EBV LMP2A	Miltenyi Biotec	Cat#130-093-615
PepTivator EBV EBNA-1	Miltenyi Biotec	Cat#130-093-613
PepTivator AdV5 Hexon	Miltenyi Biotec	Cat#130-093-495

RESOURCE AVAILABILITY

Lead contact

Further information and requests for resources and reagents should be directed to and will be fulfilled by the lead contact, Petra Bacher (p.bacher@ikmb.uni-kiel.de).

Materials availability

This study did not generate new unique reagents.

Data and code availability

- TCR sequencing data generated during this study are provided in Table S3.
- This paper does not report original code.
- Any additional information required to reanalyze the data reported in this paper is available from the lead contact upon request.

EXPERIMENTAL MODEL AND SUBJECT DETAILS

Blood donors

Vaccine blood donors were recruited following approvals by the Institutional Review Board of UKSH Kiel (identifier D409/21) and Lübeck (identifier IRON AZ 15–304). SARS-CoV-2 naïve vaccinees were enrolled between December 2020 and July 2021. Convalescent COVID-19 patients were enrolled between April and September 2020 (ethics committee of the UKSH Kiel (Identifier D474/20); University Hospital Frankfurt (Identifier 11/17); University of Cologne (Identifier 20–1295; 08–160) (Bacher et al., 2020). All blood donors signed informed consents. See Table S2 for demographic information on vaccine blood donors.

Vero cells

A Vero cell-based virus-neutralization test (cVNT) was used for measurement of SARS-CoV-2-neutralizing antibodies (see below). Vero cells (CLS Cell Lines Service GmbH, Eppelheim, Germany, order no. 605372) were incubated at 37°C, 5% CO^2 and 90% humidity in Dulbecco's modified Eagle's medium supplemented with 10 % (v/v) fetal calf serum, 3.7 g/L $NaHCO_3$, 4.5 g/L glucose, 2mM L-glutamine, and 1% (v/v) of Pen-Strep-Fungi mix containing 10,000 U/ml penicillin, 10 mg/mL streptomycin, and 25 μg/mL amphotericin B (all reagents from Bio&SELL GmbH, Feucht, Germany).

METHOD DETAILS

Antigens

Pools of lyophilized 15-mer peptides with 11–amino acid overlap, covering the complete protein sequence were purchased from JPT (Berlin, Germany): SARS-CoV-2 spike, 229E spike, OC43 spike, HKU1 spike, NL63 spike and Miltenyi Biotec (Bergisch Gladbach, Germany): Influenza A H1N1 (HA, MP1, MP2, NP and NA), CMV (pp65, IE-1), EBV (EBNA1, BZLF1, LMP2A, LMP1), AdV (Hexon). Peptides covering the sequence regions of the SARS-CoV-2 omicron variant B.1.1.529 BA.1 and the corresponding wildtype peptides were obtained from peptides&elephants (Hennigsdorf, Germany).

Peptides were resuspended according to manufacturers' instructions and cells were stimulated at a concentration of 0.5 μg/peptide/ml until otherwise indicated in the figures and figure legends. Tetanus-toxoid was purchased from Statens Serum Institute and used at a concentration of 10 μg/mL.

Antigen-reactive T cell enrichment (ARTE)

Peripheral blood mononuclear cells were freshly isolated from EDTA blood on the day of blood donation by density gradient centrifugation (Biocoll; Biochrom, Berlin, Germany). Antigen-reactive T cell enrichment (ARTE) was performed as previously described

(Bacher et al., 2013, 2016, 2019, 2020). In brief, 1-2×10e7 PBMCs were plated in RPMI-1640 medium (GIBCO), supplemented with 5% (v/v) human AB-serum (Sigma Aldrich, Schnelldorf, Germany) at a cell density of 1 × 10e7 PBMCs/2 cm^2 in cell culture plates and stimulated for 7 h in presence of 1 μg/mL CD40 and 1 μg/mL CD28 pure antibody (both Miltenyi Biotec, Bergisch Gladbach, Germany). 1 μg/mL Brefeldin A (Sigma Aldrich) was added for the last 2 h.

Cells were labeled with CD154-Biotin followed by anti-Biotin (CD154 MicroBead Kit, Miltenyi Biotec) and magnetically enriched by two sequential MS columns (Miltenyi Biotec). Surface staining was performed on the first column, followed by fixation and intracellular staining on the second column. Frequencies of antigen-specific T cells were determined based on the cell count of $CD154^+$ T cells after enrichment, normalized to the total number of $CD4^+$ T cells applied on the column. For each stimulation, $CD154^+$ background cells enriched from the non-stimulated control were subtracted.

Flow cytometry

Cells were stained in different combinations of fluorochrome-conjugated antibodies (see Key resources table). Viobility 405/520 Fixable Dye (Miltenyi Biotec) was used to exclude dead cells. For intracellular staining cells were fixed and permeabilized with the Inside stain Kit (Miltenyi Biotec). Data were acquired on a LSR Fortessa (BD Bioscience, San Jose, CA, USA). Screening of expanded T cell lines on 384-well plates was performed on a MACSQuantX Analyzer (Miltenyi Biotec). FlowJo (Treestar, Ashland, OR, USA) software was used for analysis.

Quantification of SARS-CoV-2 spike-specific antibodies

Serum antibodies were measured as described previously (Geisen et al., 2021a, 2021b). Briefly, SARS-CoV-2 S1 IgG antibodies were measured according to the manufacturer's instructions (QuantiVac, Euroimmun, Lübeck, Germany). Samples with antibody values above the highest standard (384 BAU/ml) were diluted (1:10 or 1:20) and re-analyzed. SARS-CoV-2 Nucleocapsid-protein IgG antibodies were measured using the AESKULISA SARS-CoV-2 NP IgG test.

Measurement of SARS-CoV-2-neutralizing antibodies

Dilutions of each serum were tested in duplicate in an in-house 96-well format Vero cell-based virus-neutralization test (cVNT) (Neumann et al., 2021; Rose et al., 2022a, 2022b). In brief, 2.5 × 10^4 Vero cells (order no. 605372, CLS Cell Lines Service GmbH, Eppelheim, Germany) were seeded per well and incubated at 37°C under standard conditions. On the next day, sera were heat-inactivated (56°C for 30 min) and diluted (1:10 to 1:1280) in supplemented Dulbecco's modified Eagle's medium. Then, 25 μL of the serum dilution were mixed with 25 μL of virus suspension containing 50 plaque-forming units (pfu) of an own pre-VOC B.1 strain. This virus was isolated from the upper respiratory tract of a 2020 COVID-19 patient, as previously described (Stromer et al., 2020b). The resulting 50 μL were incubated for 1 h at 37°C. Vero cells were washed with PBS, combined with 50 μL of the virus-serum dilutions and incubated for one hour on a shaker at room temperature. Thereafter, 50 μL of fresh cell culture medium supplemented with 20% fetal calf serum (v/v) was added per well and plates were incubated for four days under standard conditions. Then, cells were fixed with paraformaldehyde and stained with crystal violet. The cytopathic effect formation was compared with an untreated cell control (medium only, negative) and a viral control (50 pfu, positive) (Neumann et al., 2021; Stromer et al., 2020a). The geometric mean of the duplicates was calculated as titers.

Surrogate neutralizing antibodies (Figure S1G) were measured using a surrogate virus neutralization test (cPASS, Medac, Wedel, Germany, or BMS2326, Invitrogen, Vienna, Austria). For the comparison of the tests, samples were measured in parallel on both ELISAs and the incubation time of the thermo test was adjusted accordingly. IgG values above 35,6 BAU/ml and neutralization above 30% were considered as positive, according to the manufacturer's recommendation.

Expansion and re-stimulation of antigen-reactive T cells

For expansion of antigen-specific T cell lines, PBMCs were stimulated for 6 h, $CD154^+$ cells were isolated by MACS and further purified by FACS sorting on a FACS Aria Fusion (BD Bioscience, San Jose, CA, USA) based on dual expression of CD154 and CD69. Purified $CD154^+$ T cells were expanded in presence of 1:100 autologous antigen-loaded irradiated feeder cells in TexMACS medium (Miltenyi Biotec), supplemented with 5% (v/v) human AB-serum (GemCell), 200 U/ml IL-2 (Proleukin; Novartis, Nürnberg, Germany), and 100 IU/mL penicillin, 100 μg/mL streptomycin, 0.25 μg/mL amphotericin B (Antibiotic Antimycotic Solution, Sigma Aldrich) at a density of 2.5 × 10e6 cells/cm^2. During expansion for 2–3 weeks, medium was replenished and cells were split as needed.

For re-stimulation, fastDCs were generated from autologous $CD14^+$ MACS isolated monocytes (CD14 MicroBeads; Miltenyi Biotec) by cultivation in X-Vivo™15 medium (BioWhittaker/Lonza), supplemented with 1000 IU/mL GM-CSF and 400 IU/mL IL-4 (both Miltenyi Biotec). Before re-stimulation expanded T cells were rested in RPMI-1640 supplemented with 5% human AB-serum without IL-2 for 2 days. 0.5-1×10e5 expanded T cells were plated with fastDCs in a ratio of 1:1 of in 384-well flat bottom plates and re-stimulated for 6 h, with 1 μg/mL Brefeldin A (Sigma Aldrich) added for the last 4 h.

Analysis of functional avidity

For determining the functional avidity, *in vitro* expanded SARS-CoV-2-specific T cells were re-challenged with decreasing antigen concentrations (0.5, 0.25, 0.01, 0.025, 0.0025, 0.001, 0.00025 μg/peptide/ml) and analyzed for re-expression of CD154 and cytokines. Antigen concentrations required for half-maximal response (EC50 values) were calculated from dose-response curves using GraphPad PRISM. These curves were plotted as a semi-logarithmic plot, where the amount of antigen is plotted (on the X axis) as the

log of antigen concentration and the response is plotted (on the Y axis) using a linear scale. To compare the EC50 values of different donors, the bottom and top of the curve were defined as 0 and 100%, respectively.

T cell receptor (TCR) sequencing

For TCR sequencing, 5x10e7 PBMCs pre-vaccination and 1-2x10e7 PBMCs post-vaccination were stimulated with the spike peptide pool for 6h. $CD154^+$ cells were magnetically enriched and further purified by FACS sorting on a FACS Aria Fusion (BD Bioscience, San Jose, CA, USA) based on dual expression of CD154 and CD69. A maximum of 1x10e4 $CD154^+$ cells were analyzed. To increase the sensitivity of the used TCR profiling kit, based on 5′ RACE and switch oligo approaches, Jurkat cells were spiked into samples with less than 1x10e4 $CD154^+CD69^+$ cells. RNA was isolated using the RNeasy Micro Kit (Qiagen). TCR libraries were prepared using human TCR profiling kit (MiLaboratory), according to the manufacturer's protocol. In detail, 21 PCR cycles were used for the 1^{st} PCR and 15 cycles for the 2^{nd} PCR amplification.

Libraries were produced for n = 37 individuals for a total of n = 111 samples, i.e. 3 time points (baseline, post 1^{st} vaccination, post 2^{nd} vaccination) for each individual. Libraries were pooled equimolarly and sequenced on an Illumina NovaSeq6000 machine, SP v1.5 flow cell and 300 cycles. Data of both TCRα and β chains were obtained.

TCR repertoire analyses

PCR and sequencing error correction were performed through identification and selection of unique molecular identifiers using the software MiGEC, version 1.2.6 (Shugay et al., 2014). Filtered sequences were aligned on a TCR gene reference, clonotypes were identified, grouped and CDR3 sequences were identified using the software MiXCR version 3.0.14 (Bolotin et al., 2015). Clonotype tables containing clonotype counts, frequencies, CDR3 nucleotide and amino acid sequences and V(D)J genes were obtained and used for further analysis.

The Jurkat TCRs were then excluded from further analysis. The presence and abundance of baseline clonotypes was evaluated at 1^{st} and 2^{nd} post-vaccination time points. Pre-existing clonotypes were defined as clonotypes present both at baseline and at post-vaccination. Newly arising clonotypes post 1^{st} vaccination were defined as clonotypes present in both post-vaccination time points. Newly arising clonotypes post 2^{nd} vaccination were defined as clonotypes detected only after 2^{nd} vaccination. Overlap among baseline clonotypes and the most abundant 100 clonotypes after 2^{nd} vaccination was analyzed.

Diversity profiles of the TCRβ repertoire were evaluated for all time points using Rényi diversity profiles (Rényi, 1961). By varying the α parameter, different diversity indices are calculated: at α = 0, 1, 2 and infinite, the profiles provide the logarithm of richness, the Shannon diversity, the reciprocal Simpson diversity, and the Berger-Parker index, respectively. This means that the sample with the highest value at α = 0 has the highest richness, but that the lower value at α = infinite indicates higher proportion of the most abundant sequence. A sample with a profile that is overall higher than the profiles of other samples is more diverse, i.e. has more different clonotypes.

TCR similarity analyses

TCR similarity clusters were identified using the TCRdist algorithm of the CONGA software v0.1.1 (Schattgen et al., 2022) on the single TCRα and TCRβ chains separately. The TCRdist threshold for cluster identification for beta chain was set to 20 and for alpha to 15. An igraph object was created with the igraph package (Csardi and Nepusz, 2006), and greedy clustering was applied. Network plots were created with Gephi (Bastian et al., 2009) and Biorender showing the biggest TCR clusters, defined as clusters including a minimum of 20 unique TCRs.

QUANTIFICATION AND STATISTICAL ANALYSIS

Statistical parameters including the exact value of n, the definition of center, dispersion and precision measure, and statistical significance are reported in the Figures and the Figure Legends. Statistical tests were performed with GraphPad PRISM software 9.3 (GraphPad Software, La Jolla, CA, USA). Statistical tests were selected based on appropriate assumptions with respect to data distribution and variance characteristics, p values <0.05 were considered statistically significant.

Software

Flow cytometry data were analyzed using FlowJo (Treestar, Ashland, OR, USA) software. Graphics and statistics were created with GraphPad PRISM software version 9.3.1. (GraphPad Software, La Jolla, CA, USA). Heatmaps were generated using Genesis software, version 1.7.7 (Sturn et al., 2002). For TCR sequence analyses the software MiGEC version 1.2.6 (Shugay et al., 2014), and MiXCR version 3.0.14 (Bolotin et al., 2015) were used to obtain clonotype tables. For downstream analyses the R software v4.1.2 was used. To calculate the diversity measures the R packages vegan (Oksanen et al., 2019) and ineq (Zeileis, 2014) were used. Ggplot2 (Wickham, 2016) was used for visualization.

Immunity, Volume *55*

Supplemental information

The pre-exposure SARS-CoV-2-specific T cell repertoire determines the quality of the immune response to vaccination

Carina Saggau, Gabriela Rios Martini, Elisa Rosati, Silja Meise, Berith Messner, Ann-Kristin Kamps, Nicole Bekel, Johannes Gigla, Ruben Rose, Mathias Voß, Ulf M. Geisen, Hayley M. Reid, Melike Sümbül, Florian Tran, Dennis K. Berner, Yascha Khodamoradi, Maria J.G.T. Vehreschild, Oliver Cornely, Philipp Koehler, Andi Krumbholz, Helmut Fickenscher, Oliver Kreuzer, Claudia Schreiber, Andre Franke, Stefan Schreiber, Bimba Hoyer, Alexander Scheffold, and Petra Bacher

Figure S1

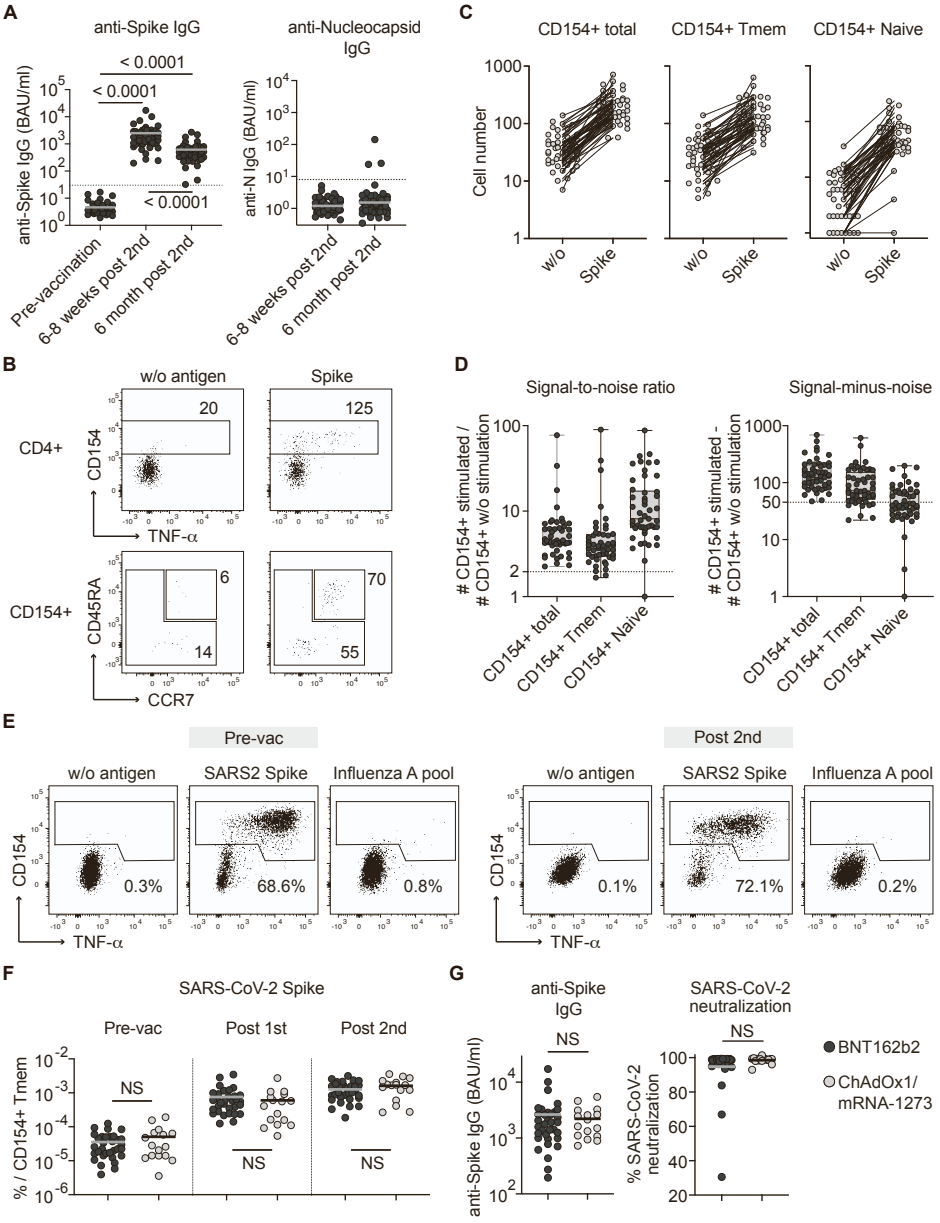

Figure S1. Specificity of CD154⁺ T cells and comparison of vaccination regimens, Related to Figure 1.

(A) Serum anti-spike and anti-nucleocapsid IgG antibody levels pre- and post-vaccination (n=50). (B) Representative dot plot examples for the *ex vivo* detection of naïve and memory SARS-CoV-2 spike-reactive CD4⁺ T cells by ARTE pre-vaccination. Absolute cell counts after magnetic CD154⁺ enrichment from 1x10e7 PBMCs are indicated. (C) Absolute cell counts obtained by ARTE pre-vaccination for total CD154⁺ cells, CD154⁺ Tmem, and CD154⁺ naive cells (n=50). (D) Signal-to-noise ratio of the ARTE assay and signal-minus-noise cell numbers for total CD154⁺ cells, CD154⁺ Tmem, and CD154⁺ naive cells pre-vaccination (n=50). (E) SARS-CoV-2 spike-reactive CD154⁺ T cells were FACS purified pre-vaccination or post 2nd vaccination, expanded for several weeks and restimulated with SARS-CoV-2 spike or a pool of Influenza A (HA, MP1, MP2, NP, NA) antigens in the presence of autologous antigen-presenting cells. Percentage of CD154⁺TNFα⁺ cells within CD4⁺ is indicated. (F, G) Comparison of individuals receiving either two doses of the Biontech/Pfizer BNT162b2 mRNA vaccine (n=34) or a heterologous immunization with AstraZeneka ChAdOx/ Moderna mRNA-1273 (n=16). (F) Frequencies of SARS-CoV-2 spike-reactive Tmem pre- and post-vaccination and (G) serum anti-spike IgG antibody levels and surrogate neutralization activity.

Each symbol in (A, C, D, F, G) represents one donor; Horizontal lines indicate geometric mean in (A) and mean in (F, G). Box-and-whisker plots display quartiles and range in (D). Statistical differences: Friedman test with Dunn´s post hoc test in (A); two-tailed Mann-Whitney test in (F, G).

Figure S2

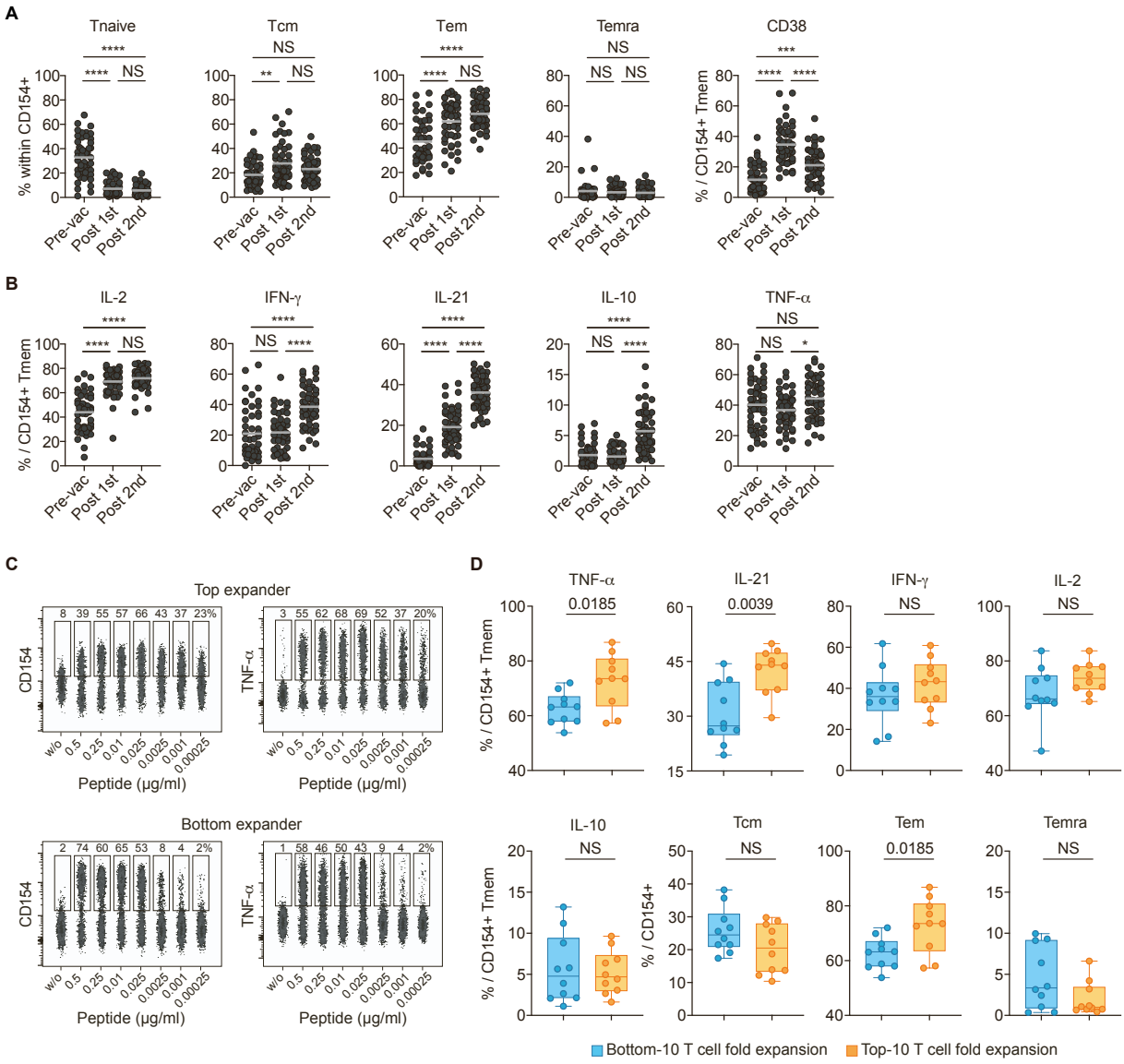

Figure S2. Characterization of vaccination-induced SARS-CoV-2 spike-reactive T cells, Related to Figure 1.

(A) *Ex vivo* phenotype of SARS-CoV-2 spike-reactive CD154$^+$ T cells. (B) *Ex vivo* cytokine production of SARS-CoV-2 spike-reactive CD154$^+$ Tmem cells. (C) Determination of EC50 values. Spike-reactive CD154$^+$ Tmem cells were FACS-purified, expanded, and re-stimulated with decreasing antigen concentration in the presence of autologous antigen-presenting cells. Representative CD154 and TNF-α staining for the indicated concentrations per peptide. Percentage within CD4$^+$ is indicated. (D) *Ex vivo* cytokine production and phenotype of SARS-CoV-2 spike-reactive CD154$^+$ Tmem cells of the bottom-10 and top-10 expander vaccinees, as determined in Figure 1E.

Each symbol in (A, B, D) represents one donor; Horizontal lines indicate mean in (A, B). Box-and-whisker plots display quartiles and range in (D). Statistical differences: Kruskal-Wallis test with Dunn's post hoc test in (A, B), two-tailed Mann-Whitney test in (D). Significant differences: ****P<0.0001; ***P<0.001; **P<0.01; *P<0.5. Tcm = central memory; Tem = effector memory; Temra = terminal differentiated effector memory.

Figure S3

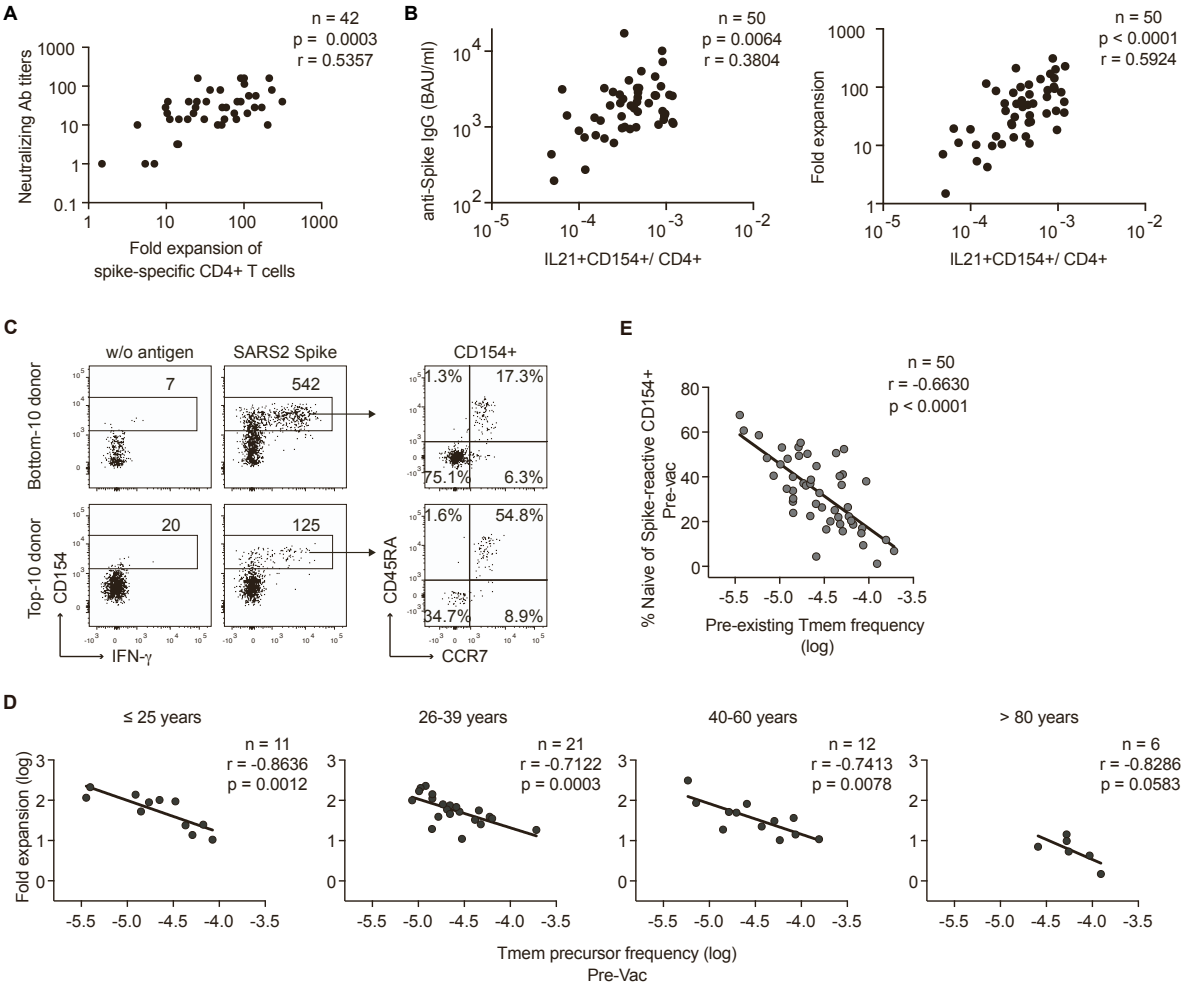

Figure S3. Correlations between fold expansion, antibody levels, IL-21 production and pre-existing Tmem frequencies, Related to Figures 1-3.

(A) Spearman correlation of the fold expansion of spike-reactive $CD4^+$ T cells and neutralizing antibody titers measured 6-8 weeks post 2^{nd} vaccination. (B) Spearman correlation of spike-reactive IL-21 producers and anti-spike IgG titers (left plot) or the fold expansion of spike-reactive $CD4^+$ T cells (right plot) post 2^{nd} vaccination. (C) Representative dot plot examples for the *ex vivo* detection of SARS-CoV-2 spike-reactive T cells pre-vaccination of a bottom-10 and top-10 donor. (Left) Absolute cell counts of $CD154^+$ cells after magnetic enrichment from 1x10e7 PBMCs and (right) percentage of naïve, Tcm, Tem and Temra cells within $CD154^+$ are indicated. (D) Spearman correlation between the frequencies of spike-reactive Tmem pre-vaccination (x-axis) and the fold expansion post 2^{nd} vaccination (y-axis) for individual age groups. (E) Spearman correlation between the frequencies of spike-reactive Tmem pre-vaccination (x-axis) and the proportion of spike-reactive naïve T cells pre-vaccination (y-axis).

Each symbol in (A, B, D, E) represents one donor. Tcm = central memory; Tem = effector memory; Temra = terminal differentiated effector memory.

Figure S4

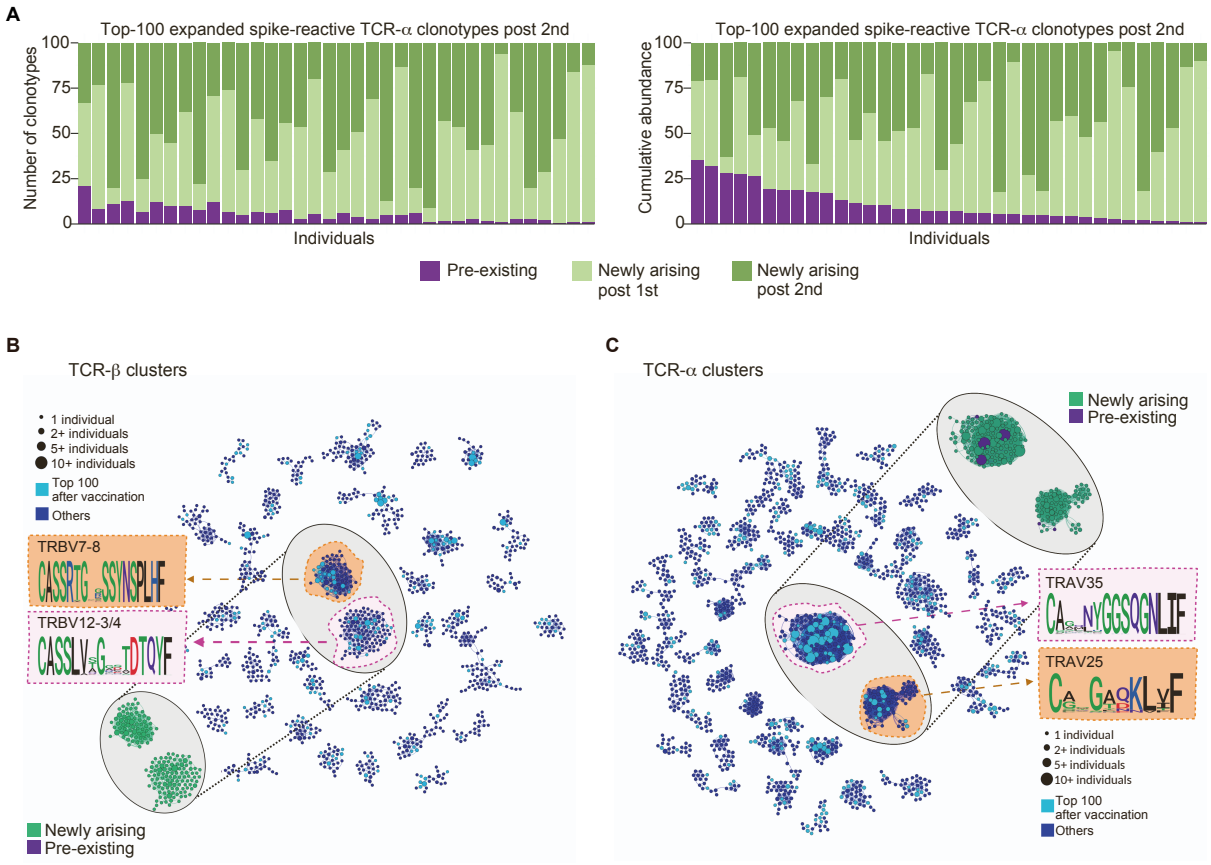

D

AaVJ	Number of individuals with identified sequence # (% of total)	Number of individuals with pre-existing sequence # (% of identified)	Number of individuals with newly arising sequence # (% of identified)
CAASLYGGSQGNLIF_TRAV35_TRAJ42	2 (5.4%)	1 (50%)	1 (50%)
CAGLNYGGSQGNLIF_TRAV35_TRAJ42	34 (91.9%)	4 (11.8)	30 (88.2%)
CAGQNYGGSQGNLIF_TRAV35_TRAJ42	35 (94.6%)	2 (5.7%)	33 (94.3%)
CAGRNYGGSQGNLIF_TRAV35_TRAJ42	28 (72.9%)	1 (3.57%)	1 (96.4%)

Figure S4. TCR sequence and similarity analyses, Related to Figure 4.
(A) Analysis of the top 100 expanded TCRα spike-reactive clonotypes post 2nd vaccination. The number of clonotypes (left graph) and their cumulative relative abundance (right graph) derived from the pre-existing, post 1st or post 2nd newly arising vaccination repertoire is indicated. Each bar represents one donor (n=37).
(B, C) Network of clonotypes similarity clusters. TCRβ (B) and TCRα (C) sequences were grouped based on their CDR3 amino acid sequence similarity using the TCRdist algorithm and Gephi for visualization (see STAR methods). Each dot represents one clonotype, the size of the dots indicates in how many individuals they were detected. The distance between the dots indicates the similarity of the TCR sequences. Colors indicate whether clonotypes were found in the top 100 post-2nd vaccination repertoire (light blue) or not (dark blue).
For the biggest two similarity clusters, a zoom view is shown, indicating the used TCR motif. Clonotypes that are newly arising post-vaccination are indicated in green, clonotypes that were also found in the pre-vaccination repertoire in individual donors are depicted in purple.
(D) For TCRα clonotypes that were also identified in the pre-existing repertoire (Figure S4C purple) the number of individuals where they were pre-existing or newly arising is shown in the table.

Figure S5

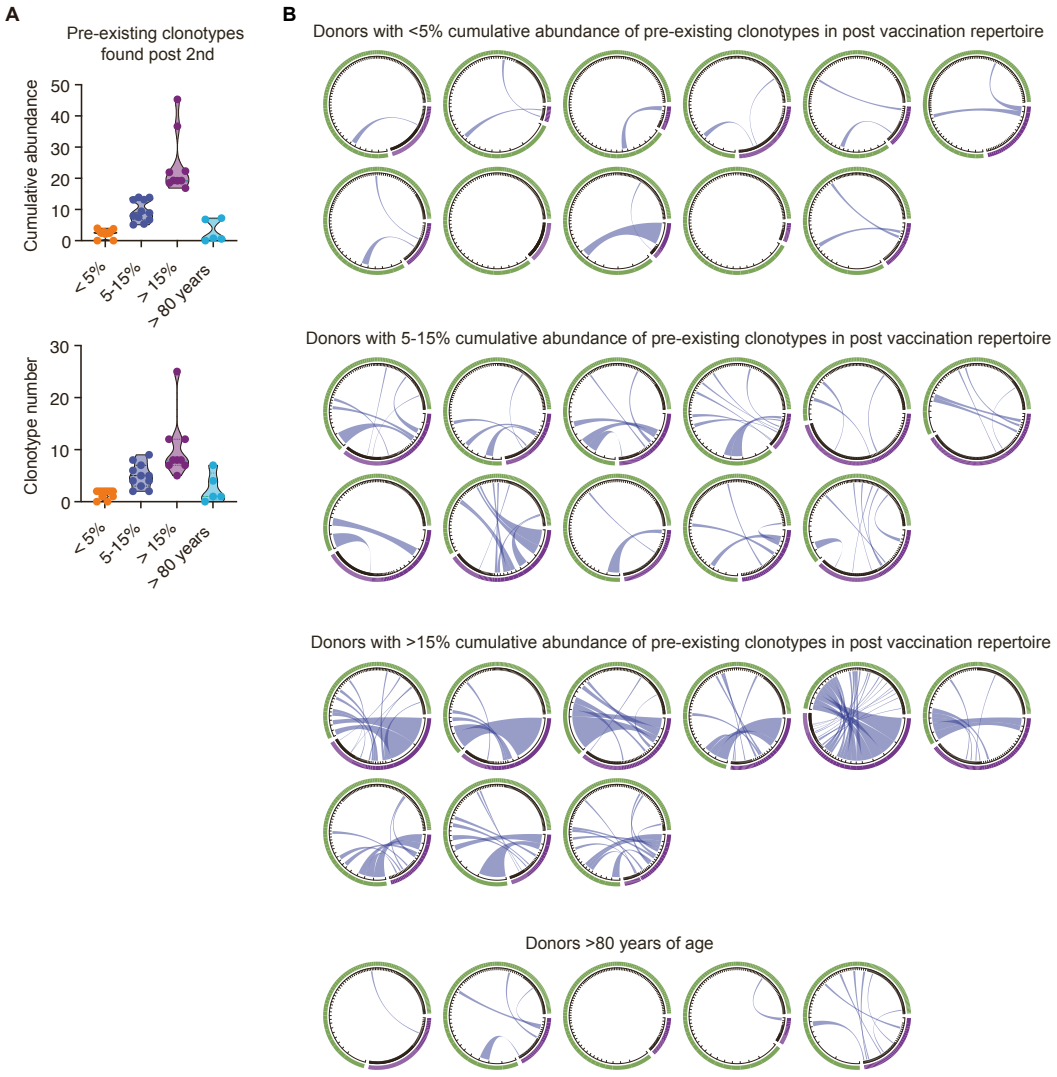

Figure S5. Clonal fates of pre-existing clonotypes post-vaccination, Related to Figure 4.
(A) Donors were grouped according to the cumulative abundance of pre-existing clonotypes in the top-100 post vaccination repertoire (<5%, 5-15%, >15%; donors >80 years of age were analyzed as separate group). Bottom: number of pre-existing clonotypes found in the post vaccination repertoire for each bin. Truncated violin plots with quartiles and range are shown.
(B) Donors were grouped as in Figure S5A. Each circos plot represents the TCRβ sequences of the detected clonotypes pre-vaccination (purple) and the top-100 clonotypes post 2nd vaccination (green) of one donor. Connecting lines show TCRβ sequences that are present at both time points.

Figure S6

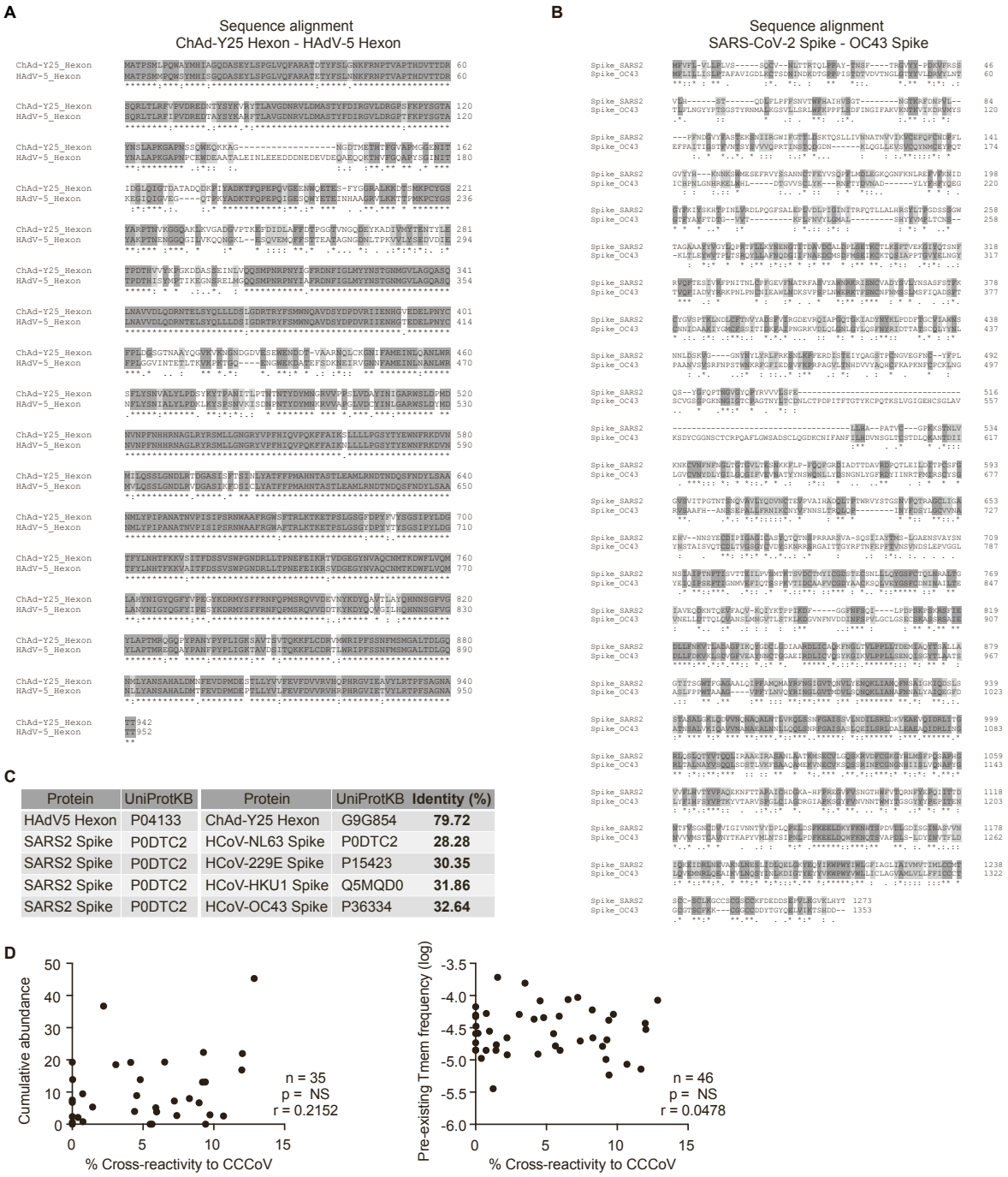

Protein	UniProtKB	Protein	UniProtKB	**Identity (%)**
HAdV5 Hexon	P04133	ChAd-Y25 Hexon	G9G854	**79.72**
SARS2 Spike	P0DTC2	HCoV-NL63 Spike	P0DTC2	**28.28**
SARS2 Spike	P0DTC2	HCoV-229E Spike	P15423	**30.35**
SARS2 Spike	P0DTC2	HCoV-HKU1 Spike	Q5MQD0	**31.86**
SARS2 Spike	P0DTC2	HCoV-OC43 Spike	P36334	**32.64**

Figure S6. Sequence alignments and cross-reactivity to CCCoVs, Related to Figure 6.
(A, B) Clustal Omega sequence alignment. Identical and similar amino acids are indicated in dark and light gray, respectively. (A) Sequence alignment of the hexon proteins of the chimpanzee adenovirus Y25 (ChAd-Y25) used as a vector for ChAdOx1 and human adenovirus C serotype 5 (HAdV-5). (B) Sequence alignment of the spike proteins of SARS-CoV-2 and the human Betacoronavirus OC43. (C) Percentage of sequence identities based on Clustal Omega sequence alignment. (D) SARS-CoV-2 spike-reactive T cells were expanded post vaccination and restimulated with a pool of CCCoV spike proteins. The percentage of cross-reactivity to CCCoVs was calculated based on the reactivity to the CCCoVs spike pool in relation to total reactivity against SARS-CoV-2 spike. Spearman correlations of the cross-reactivity to CCCoV and (left): the cumulative abundance of pre-existing clonotypes contributing to the post-vaccination response; (right): the frequency of pre-existing spike-specific memory cells pre-vaccination. Each symbol in (D) represents one donor.

Table S1. Cohort characteristics, Related to STAR Methods and Figures 1-6.

		SARS-CoV-2 naïve vaccinees[1]	COVID-19 patients[2]	
			Mild	Severe
Number of individuals		50	32	14
Age (mean ± SD, years)		40 ± 20.2	44.6 ± 15.2	64.2 ± 8.2
Gender	Male (N, %)	20 (40%)	13 (40.6%)	10 (71.4%)
	Female (N, %)	30 (60%)	19 (59.4%)	4 (28.6%)
Vaccination regimen	BNT162b2 – BNT162b2 (N, %)	34 (68%)	NA	NA
	ChAdOx1 – mRNA-1273 (N, %)	16 (32%)	NA	NA
COVID-19 WHO classification		NA	WHO 1+2	WHO 4-7

NA = Not applicable.

[1]All vaccinees were tested negative for SARS-CoV-2 IgG (QuantiVac, Euroimmun, Lübeck, Germany) before inclusion into the study.

[2]All patients were tested positive for SARS-CoV-2 antibodies (Elecsys Anti-SARS-CoV-2 IgG/IgM Roche Diagnostics GmbH or anti-SARS-CoV-2 IgG ELISA, Euroimmun, Lübeck, Germany); all but five mild COVID-19 cases were tested positive for SARS-CoV-2 RNA. We included 5 mild cases of COVID-19 without positive SARS-CoV2 RNA test, who had a positive antibody test, clinical symptoms suggestive of COVID-19 and a traceable contact person found positive. None of the COVID-19 patients had active disease at the time point of measurement. The COVID-19 severity was assessed based on WHO ordinal scale (https://www.who.int/publications/i/item/covid-19-therapeutictrial-synopsis; severe COVID-19 cases: WHO4 n=4; WHO5 n=2; WHO6 n=3; WHO7 n=5).

Table S2. Demographic information for vaccination study participants, Related to STAR Methods and Figures 1-6.

Patient ID	Sample ID_TCR seq	Age	Gender	Vaccination regimen	Health care worker
ID_1	TCR_1	26	male	BNT162b2 - BNT162b2	Yes
ID_3	TCR_2	57	female	BNT162b2 - BNT162b2	Yes
ID_4	TCR_3	40	male	BNT162b2 - BNT162b2	Yes
ID_5	TCR_4	25	female	BNT162b2 - BNT162b2	Yes
ID_6	TCR_5	40	male	BNT162b2 - BNT162b2	Yes
ID_7	TCR_6	25	female	BNT162b2 - BNT162b2	Yes
ID_8	TCR_7	34	female	BNT162b2 - BNT162b2	Yes
ID_9	TCR_8	24	female	BNT162b2 - BNT162b2	Yes
ID_10	ND	27	female	BNT162b2 - BNT162b2	Yes
ID_11	TCR_9	25	female	BNT162b2 - BNT162b2	Yes
ID_12	TCR_10	27	female	BNT162b2 - BNT162b2	Yes
ID_13	TCR_11	23	female	BNT162b2 - BNT162b2	Yes
ID_14	ND	51	female	BNT162b2 - BNT162b2	Yes
ID_15	TCR_12	33	female	BNT162b2 - BNT162b2	Yes
ID_16	TCR_13	30	male	BNT162b2 - BNT162b2	Yes
ID_17	TCR_14	41	female	BNT162b2 - BNT162b2	Yes
ID_18	TCR_15	45	female	BNT162b2 - BNT162b2	Yes
ID_19	TCR_16	37	female	BNT162b2 - BNT162b2	Yes
ID_20	TCR_17	38	male	BNT162b2 - BNT162b2	Yes
ID_21	TCR_18	37	female	BNT162b2 - BNT162b2	Yes
ID_22	TCR_19	35	male	BNT162b2 - BNT162b2	Yes
ID_23	TCR_20	22	male	BNT162b2 - BNT162b2	Yes
ID_24	ND	26	female	BNT162b2 - BNT162b2	Yes
ID_25	ND	22	male	BNT162b2 - BNT162b2	Yes
ID_26	ND	84	female	BNT162b2 - BNT162b2	No
ID_28	ND	86	female	BNT162b2 - BNT162b2	No
ID_29	TCR_21	44	male	BNT162b2 - BNT162b2	Yes
ID_30	TCR_22	54	male	BNT162b2 - BNT162b2	Yes
ID_31	TCR_26	81	male	BNT162b2 - BNT162b2	No
ID_32	TCR_27	83	male	BNT162b2 - BNT162b2	No
ID_33	TCR_28	83	male	BNT162b2 - BNT162b2	No
ID_34	TCR_31	33	female	ChAdOx1 - mRNA-1273	No
ID_35	TCR_32	28	female	ChAdOx1 - mRNA-1273	No
ID_36	TCR_33	21	female	ChAdOx1 - mRNA-1273	No
ID_37	TCR_34	42	female	ChAdOx1 - mRNA-1273	No
ID_38	TCR_35	32	female	ChAdOx1 - mRNA-1273	No
ID_39	TCR_36	30	female	ChAdOx1 - mRNA-1273	No
ID_40	TCR_37	36	female	ChAdOx1 - mRNA-1273	No
ID_41	TCR_38	54	male	ChAdOx1 - mRNA-1273	No
ID_42	ND	32	male	ChAdOx1 - mRNA-1273	No
ID_43	ND	44	male	ChAdOx1 - mRNA-1273	No
ID_44	ND	29	female	ChAdOx1 - mRNA-1273	No
ID_45	ND	31	female	ChAdOx1 - mRNA-1273	No
ID_46	ND	58	male	ChAdOx1 - mRNA-1273	No
ID_47	ND	30	female	ChAdOx1 - mRNA-1273	No
ID_48	ND	24	female	ChAdOx1 - mRNA-1273	No
ID_49	ND	29	male	ChAdOx1 - mRNA-1273	No
ID_50	TCR_40	9	male	BNT162b2 - BNT162b2	No
ID_51	TCR_39	7	female	BNT162b2 - BNT162b2	No
ID_53	TCR_29	82	male	BNT162b2 - BNT162b2	No
ID_54	TCR_30	82	female	BNT162b2 - BNT162b2	No